university of groningen / faculty of science and engineering

Passive hydrodynamic imaging using the pressure amplitude and flow velocity

Performing object localization with an Extreme Learning Machine

Gabriel-Vlad Păun, s3811816, g.v.paun@student.rug.nl,
Supervisors: Prof Dr S. M. van Netten & Dr B. J. Wolf

Abstract:

Lateral lines are sensor arrays designed to detect objects moving through fluids. They possess distinct advantages compared to other types of sensors, being undetectable, usable in low light conditions and suitable for short-range detection. This study investigated whether the addition of hydrodynamic pressure sensors to a velocity-sensitive 2D lateral line can improve the accuracy of object localisation. An extreme learning machine (ELM) was trained on simulated data generated by placing a vibrating sphere along different grid points on a 2D map. Multiple configurations of lateral lines were tested, by gradually increasing the number of pressure sensors and decreasing the number of velocity sensors, and gradually pulling the y sensors away from the x sensors. The ELM learned to output the position and direction of vibration of the simulated sphere. Two different methods of positioning the velocity sensors relative to the pressure sensors were compared, one where both are located along a single horizontal line, and one where the velocity sensors are placed on top of the pressure sensors, on a vertical line, forming the shape of an upside-down T. It was found that pressure sensors can be used to replace some of the velocity sensors is a 2D lateral line; for determining the position of an object, few velocity sensors are required. However, determining the direction of vibration was seen to require at least as many velocity sensors as pressure sensors.

1 Introduction

Artificial lateral lines (ALLs) are short-range sensory systems for underwater navigation and object localization based on hydrodynamics, i.e. on fluid flow, and are inspired by an organ found in fish. Moving objects generate a flow field, which can be detected passively (without active input) by ALLs. In addition, when attached to a moving body, the lateral line can be used to detect obstacles by sensing the flow field generated by the body it is attached to, and detecting the reverberations of the flow that return after impacting an obstacle. This form of hydrodynamic imaging is active, because it depends on the active input of the observer. In fish, the lateral line plays a role in mating, predator avoidance, and schooling, among others (Bleckmann & Zelick, 2009).

The lateral line organ found in fish encodes the velocity and pressure gradient profiles of the flow in a line along the body of the fish. This organ consists of flow sensitive organelles known as neuromasts, of which there are two types: superficial neuromasts (SNs), located on the body of the fish, and canal neuromasts (CNs), located underneath the scales. SNs encode the parallel velocity flow, whereas CNs encode the pressure gradient, and simultaneously also the acceleration, as the two are proportional (Netten & McHenry, 2013; Curcic-Blake & van Netten, 2006).

When used for passive detection, ALLs possess the advantage of being covert and not requiring light to function; they can be used in low-light conditions, deep underwater, such as on the ocean floor, and for stealthily monitoring schools of fish. They can also be mounted on stationary platforms in harbours to help ships dock.

1.1 State of the art

A number of different methods are known for passive sensing using the sensor data from an ALL. Curcic-Blake and van Netten (2006) presented an algorithm dubbed the continuous wavelet transform (CWT) based on the observation that the flow potential can be analyzed in terms of wavelets. In

their original paper, they decomposed the flow velocity parallel to the sensory array into a weighted sum of two wavelets; this was later extended in Wolf (2020) for the flow velocity orthogonal to the lateral line. Each wavelet is also multiplied by a factor dependent on the direction of movement of the source. The quadrature method (Bot, Wolf, & van Netten, 2021) for 2D-sensitive velocity sensors builds a curve from the two components of the flow velocity that is "nearly independent of the orientation" of the source, thus estimating the distance. The orientation can then be estimated from the position and velocity by using the wavelet-based description of the velocity, as described above.

In addition, Boulogne, Wolf, Wiering, and van Netten (2017) tested three different neural network architectures for 1D sensitive ALLs: an extreme learning machine, an echo state network, and a multi-layer perceptron. The extreme learning machine was able to solve the localization problem with higher accuracy in a high signal-to-noise ratio (SNR) than the other two.

Compared to other types of algorithms, neural networks possess the advantages of requiring less domain specific knowledge to implement, and, due to their statistical nature, may be more generalizable than other algorithms.

Wolf (2020) used an extreme learning machine with 2D-sensitive velocity sensors, which improved the accuracy compared to Boulogne et al. (2017). The neural network exhibited different errors for position and orientation, implying that the task of position and orientation detection should be separated by e.g. using one neural network for each.

Of the methods described above, none have used pure pressure sensors. Pressure gradient sensors have been used for ALLs, as these are analogous to the canal neuromasts found in the fish lateral line; the pressure gradient is proportional to the acceleration, and so pressure gradient sensors are essentially acceleration sensors.

1.2 Aims of this study

This study aims to train a neural network to perform hydrodynamic imaging skillfully, without overfitting, on a simulated data set. The data will be generated using the grid strategy described by Wolf and van Netten (2019), with a dipole vibrating harmonically with a known frequency and amplitude. Many different combinations of pressure and velocity sensors are tested, to determine the optimal configuration for use in a lateral line.

Where this does break from previous research is by utilizing the pressure amplitude, alongside the 2D velocity. Other studies have utilized the pressure differential, for example by building two parallel pressure-sensitive arrays and calculating the gradient from the measurements (as in Venturelli et al. (2012)). The pressure gradient is encoded in the fish lateral line by CNs, and is proportional to the acceleration field.

1.3 Structure of the Paper

In the Background section, we describe the conceptual background behind the Extreme Learning Machine, the theory of how this type of neural network works. In addition, in this section the flow model is also described. In the Methods section, we explain how the data generation is performed, and discuss the specifics of the implementation of the neural network for this study. Furthermore, within this section, we explain the different sensor configurations used, how hyperparameter optimization is performed, and the main experimental procedure. In the Results section, we explain which hyperparameters were picked after the optimization step, and describe the performance of an ELM with different configurations of sensors. In the discussion and conclusion, we summarize the main findings and discuss possible confounding factors.

2 Background

2.1 Extreme Learning Machine

Extreme learning machines (ELMs) (Huang, Zhu, & Siew, 2006) are a type of feedforward network with a single hidden layer in which the input weights, and optionally the bias, are arbitrarily initialized and fixed at the start. Only the output weights have to be trained, and can be learned in a single step via computing the Moore-Penrose generalized inverse (also known as the pseudoinverse) of the internal state matrix.

They can be formalized according to the following equations:

$$H = f(X\ W_{\text{in}} + b) \tag{2.1}$$

$$Y = H\ W_{\text{out}} \tag{2.2}$$

Where H is the internal state matrix, f is the activation function on the hidden layer, X is the matrix of input vectors, Y is the matrix of output vectors, b is the vector of biases, and W_{in}, W_{out} are the input and output weight matrices, respectively.

The second equation can be treated as a system of linear equations with H and Y being constants and W_{out} a matrix to be computed. An approximate solution $\hat{W}_{\text{out}}$ that minimises the mean square error can be found by taking the pseudoinverse of matrix H:

$$\hat{W}_{\text{out}} = H^{\dagger}Y \tag{2.3}$$

Fast methods exist for calculating $H^{\dagger}$, based on singular value decomposition. This makes training an ELM significantly faster compared to other types of neural networks.

In addition, ELMs tend to outperform other types of neural networks in terms of accuracy (Huang et al., 2006). For hydrodynamic imaging, ELMs have exhibited higher accuracy than echo state networks and multi-layer perceptrons (Boulogne et al., 2017).

ELMs also possess the advantage of simplicity, having only two trainable hyperparameters: the size of the hidden layer and the activation function on the hidden layer. This makes hyperparameter optimization easier to do.

2.1.1 Hidden Layer Size

The hidden layer size (R) of an ELM is known to be equal to the number of observations (N) the ELM can learn (Huang et al., 2006). This can be clearly seen from the output equation of the ELM:

$$Y = H\ W_{\text{out}} \tag{2.4}$$

H, the internal state matrix, has the shape $N \times R$; each row in H corresponds to a single data point, and there are as many rows as there are data points. When $R = N$, H is a square matrix, and from the definition of the pseudoinverse, $H^{\dagger} = H^{-1}$ for invertible matrices. Therefore, $\hat{W}_{\text{out}} = W_{\text{out}}$, which means that with $R = N$, the ELM perfectly predicts the training data, and no learning takes place.

2.2 Flow Model

Lamb (1932) described the flow generated by the movement of a sphere through a fluid as a scalar velocity potential field. The velocity field is taken to be the spatial gradient of the potential. Other fields such as the acceleration and the spatial gradient of the pressure can be derived from the velocity potential.

The velocity potential ϕ at location $\vec{r}$, generated by a sphere of radius a with velocity $\vec{W}$, located in the origin, as given by Lamb (1932) is:

$$\phi = \frac{a^3}{2\|r\|^3}(\vec{W} \cdot \vec{r}) \tag{2.5}$$

The velocity field v is the spatial gradient - $\nabla_r \phi(r)$ (Franosch, Sichert, Suttner, & Hemmen, 2005). Along any axis α, the component v_α of the velocity field at location $\vec{r}$ is:

$$v_\alpha = \frac{a^3}{2\|r\|^3}[-W_\alpha + 3\frac{(\vec{W} \cdot \vec{r})}{\|r\|^2} r_\alpha] \tag{2.6}$$

When the sphere is not located in the origin but at location r_0, r_α has to be replaced by $r_\alpha - r_{0_\alpha}$, where r_{0_α} is the position of the sphere along axis α, and $\|r\|$ with $\|r_s\| = \|(\vec{r} - \vec{r_0})\|$:

$$v_\alpha = \frac{a^3}{2\|r_s\|^3}[-W_\alpha + 3\frac{(\vec{W} \cdot \vec{r})}{\|r_s\|^2}(r_\alpha - r_{0_\alpha})] \tag{2.7}$$

The equations described thus far are taken from S. van Netten (personal communication, March 3rd 2022). They were extracted from a non-publicly accessible deliverable (Deliverable 3.2) on the Lakhsmi Consortium's website by the author. This formalism is valid only when the viscosity is negligible.

In the case of a sphere vibrating with frequency f and amplitude X_0 (angular frequency $\omega = 2\pi f$), the pressure is symmetrical around the direction of vibration and can be described, in polar coordinates, as in Curcic-Blake and van Netten (2006), as:

$$p(r_s, \gamma, t) = P(r_s, \gamma)\sin(\omega t) \tag{2.8}$$

Where $P(r_s, \gamma)$ is the pressure amplitude:

$$P(r_s, \gamma) = -\frac{1}{2}\rho\omega^2\ a^3 X_0 \cos(\gamma)\frac{1}{r_s^2} \tag{2.9}$$

$\cos\gamma$ can be substituted by $\cos(\theta - \phi)$, where θ is the angle between the segment r_s and the x-axis, and ϕ is the direction of vibration. Along the x-axis ($y = 0$), this yields the substitution:

$$\cos(\theta - \phi) = \frac{(x_0 - x)\cos\phi + y_0 sin\phi}{\left[(x_0 - x)^2 + y_0^2\right]^{\frac{1}{2}}} \tag{2.10}$$

Combining the two equations leads to the following formula for pressure along the x-axis in Cartesian coordinates:

$$P(x) = \frac{\rho\omega^2 a^3 X_0}{2} \frac{\left[(x - x_0)\cos\phi - d\sin\phi\right]}{\left[(x - x_0)^2 + y^2\right]^{\frac{3}{2}}} \tag{2.11}$$

All the above is after Curcic-Blake and van Netten (2006).

3 Methods

3.1 Data Generation

Data was generated using the grid strategy, as in Wolf (2020): on a $2L$ x L map (where L is the length of the ALL), a spherical dipole vibrating with a fixed frequency $f = 1$Hz and amplitude $X_0 = \frac{1}{4\pi}$L, with the radius $a = 0.05L$ was placed on every point of a grid covering the entire map, apart from the points located within a distance lesser than 0.1L of the sensors, with the distance between any two neighbouring points on the grid being 0.1L. The frequency, amplitude and radius were arbitrarily selected. The points close to the sensors are excluded, because including them would result in the sensor array and dipole being in the same location, which is not physically possible. The set of grid points not including the ones close to the sensors is referred to as G.

At each point $\langle x, y\rangle$ in G, the dipole was oriented in 10 random directions and made to vibrate, with each direction (angle) ϕ being sampled from the uniform distribution $[0, 2\pi]$.

For each combination of position $\langle x, y\rangle$ and orientation ϕ, simulated measurements along the sensor array were taken. This raw data is then sorted by the type of sensor it is taken from (pressure or velocity sensors). Afterwards, noise is added, and then the data are normalized together with other data from the same type of sensor. v_x and v_y sensors are sorted and normalized together.

3.1.1 Noise

To each measured velocity v a noise value sampled from the uniform distribution $[-10^{-6}, 10^{-6}]$ is added, resulting in a noisy velocity v^*. This is based on Wolf, Morton, MacPherson, and Van Netten (2018), and represents a realistic amount of sensor noise. The average proportion of noise (APN) was computed for the noisy velocity measurements. The raw pressure readings p were then multiplied by 1 + APN, resulting in noise pressures p^*, causing both pressure and velocity to have the same average amount of relative noise. This was done because unlike for velocity, realistic measures of noise were not known from prior research. The two components of the velocity measurements are concatenated before the APN is calculated.

$$v = [v_\mathrm{x}; v_\mathrm{y}]^T \tag{3.1}$$

$$v^* = v + \mathrm{uniform}[-10^{-6}, 10^{-6}] \tag{3.2}$$

$$\mathrm{APN} = \frac{1}{N}\sum_{i=1}^{N} \frac{v_\mathrm{i}^* - v_\mathrm{i}}{v_\mathrm{i}^*} \tag{3.3}$$

$$p^* = p \times (1 + \mathrm{APN}) \tag{3.4}$$

In the equations above, N is the number of sensor readings in the vector of concatenated velocity measurements, i.e. $v_\mathrm{x} + v_\mathrm{y} = 2v$.

3.1.2 Normalization

The noisy measurements are then normalized separately:

$$v_\mathrm{final} = \frac{v^*}{\max(|v^*|)} \tag{3.5}$$

$$p_\mathrm{final} = \frac{p^*}{\max(|p^*|)} \tag{3.6}$$

3.1.3 Final Preprocessing

This process creates a data set with 2110 samples. Because this data set has to be split into training and testing subsets, it is randomly shuffled to ensure that as many different positions and orientations as possible are represented in both subsets. In both the hyperparameter optimization stage and the actual experiment, 10-fold cross validation is used. This means that at each iteration of the cross-validation scheme, the training set covers $2110 \times \frac{9}{10} = 1899$ samples and the testing set $2110 \times \frac{1}{10} = 211$ samples.

3.2 Neural Network

Each node in the input layer of the ELM receives data from a sensor along the lateral line. With VP configurations, there are two nodes for each 2D-sensitive velocity sensor, each node receiving as input one of the two components of the measured velocity.

Two types of activation functions are used, tanh and the rectified linear unit ReLU, the latter defined as:

$$\mathrm{ReLU}(x) = \left\{ \begin{array}{ll} x, & \text{if } x > 0 \\ 0, & \text{if } x \leq 0 \end{array} \right\} \tag{3.7}$$

The weights between the input and hidden layer are fixed from the uniform distribution [-0.5, 0.5]:

$$W_{\text{in}} = \text{uniform}[-0.5, 0.5] \tag{3.8}$$

Where each row $W_{\text{in}}(n)$ contains the input weights for the nth hidden node for every n from 0 to $R-1$, where R is the size of the hidden layer; therefore, the matrix W_{in} has shape $I \times R$, where I is the size of the input layer. The input and hidden layers both contain a bias node with a constant activation value of 1.

In the training stage, when calculating the internal matrix H of the ELM, for each data point, a different bias vector sampled from the same distribution as the velocity noise is added to the weighted input values sent to the hidden nodes:

$$H(n) = f(X(n)\ W_{\text{in}} + \text{uniform}[-10^{-6}, 10^{-6}]) \tag{3.9}$$

Where n is the index of the nth data point. This is to prevent overfitting on the training data; the noise is not included in the testing stage.

Each data point in $X(n)$ is represented as a column vector of the input matrix. After the entire state matrix H has been calculated, the output weight matrix is computed using the pseudo inverse of H: $\hat{W}_{\text{out}} = H^{\dagger}\ Y$, where Y is the output matrix, and similarly the output at data point n is packed into the nth row of the matrix. Each row of the output matrix encodes the position and orientation in the form:

$$\langle b, d, cos\phi, sin\phi \rangle \tag{3.10}$$

Where b and d are the horizontal and vertical positions, respectively, and ϕ is the direction in which the dipole is vibrating. The cosine and sine values are used instead of the angle to ensure that all the values processed and produced by the ELM are within the interval $[-1, 1]$; in addition, the sign of each of these values carries information about the relative direction of vibration of the object; the cosine determines the direction of vibration along the x-axis, and the sine determines the direction along the y-axis.

In the testing stage, the output of the network is computed as:

$$Y = f(X\ W_{\text{in}})\ \hat{W}_{\text{out}} \tag{3.11}$$

The ELM minimizes the mean square error (MSE) of the prediction, but this is an overall error value that makes it difficult to interpret the individual position and orientation errors. Therefore, when reporting the performance of the ELM, two loss function are used: the mean Euclidean distance (MED) for the position, and the mean difference between the angles (MAD) for the orientation.

$$\mathrm{MED}(Y,\ \hat{Y}) = \|Y - \hat{Y}\| \tag{3.12}$$

$$\mathrm{MAD}(\phi,\ \hat{\phi}) = \left\{ \begin{array}{ll} |\phi - \hat{\phi}|, & \text{if } |\phi - \hat{\phi}| \leq \pi \\ 2\pi - |\phi - \hat{\phi}|, & \text{if } |\phi - \hat{\phi}| > \pi \end{array} \right\} \tag{3.13}$$

The orientation errors $\mathrm{MAD}(\phi, \hat{\phi})$ are reported in degrees.

3.3 Sensor Configuration

Two types of sensors configurations, distinguished by the placement of the pressure sensors relative to the velocity sensors, were tested.

In the first configuration type, referred to as the horizontal configuration, both the pressure and the velocity sensors are located within a linear, horizontal sensor array, placed at the horizontal line at y = 0. The pressure sensors are placed first, distributed evenly along the array from $x = -0.5\mathrm{L}$ to $x = 0.5\mathrm{L}$. The distance p_i between any two neighbouring pressure sensors is equal to $\frac{1}{p-1}\mathrm{L}$, where p is the number of pressure sensors. Afterwards, the v_x sensors are distributed evenly along the array from the location of the first v_x sensor at $\mathrm{x} = -0.5\mathrm{L} + \frac{1}{10(p-1)}\mathrm{L}$ to $0.5\mathrm{L} - \frac{1}{10(p-1)}\mathrm{L}$. There are as many v_x sensors as v_y sensors, i.e. $v_\mathrm{x} = v_\mathrm{y}$. This number is varied between configurations and has the discrete range of values $[2, 30] \cap \mathbf{N}$. The number of pressure sensors p is then selected with the formula $p = 32 - v_\mathrm{x}$.

In the second configuration type, referred to as the T-configuration, the pressure sensors are placed horizontally along a line at the bottom of the grid, and the v_x are placed on a vertical line orthogonal to the midpoint of the pressure sensor array, in the shape of an upside down T. Each sensor type is distributed evenly along the line it is placed on and covers the full range of the line, having a length equal to L.

In both configurations, after these preliminary measures are taken, the v_y sensors are pulled apart from the v_x along the length of the line the sensors are placed on, according to the displacement d - which is unique for each configuration and varies from $\frac{1}{32}$, $\frac{2}{32}$... to $\frac{16}{32}$. The displacement shows the relative overlap between the v_x and v_y sensors: at $d = 0$, the v_x and v_y are right on top of each other, or, in other words, 100% of the line segments covered by v_x and v_y overlap; at $d = 0.5$, 50% of the two line segments overlap. To ensure that the lateral line has a length equal to 1, all distances between sensors are then scaled by $\frac{1}{1+d}$. In the T-configuration type, this is done solely for the array of velocity sensors. All combinations of sensor types obeying these constraints were tested. This gives in total 464 configurations for each of the two configuration types.

Graphical descriptions for two example configurations from each type are given next. In each of the figures, the sensor types are represented as large coloured circles, and the grid points in G (defined in Section 3.1) are the small black dots. Some points are described as being above others. In this context, this refers to them being located at a position y farther from $y = 0$ in the positive direction.

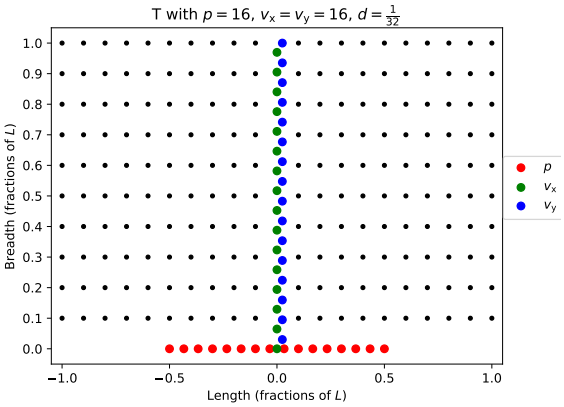

Figure 3.1: T Configuration with $p = v_\mathrm{x} = 16,\ d = \frac{1}{32}$

In Figure 3.1, the layout of the T Configuration with $p = v_\mathrm{x} = 16,\ d = \frac{1}{32}$ is shown. In this figure, it can be seen that the velocity sensors are located on a separate line from the pressure sensors, a vertical line located at x = 0. The v_y sensors are moved to the right of the v_x sensors in order to make them more distinguishable, but in fact both sensor types are located along the same vertical line. It can be seen that the v_y sensors are slightly displaced from the v_x sensors: the first v_y sensor is located at a higher y-coordinate compared to the v_x sensor. In addition, note that the grid points right in the middle of the map are excluded from G.

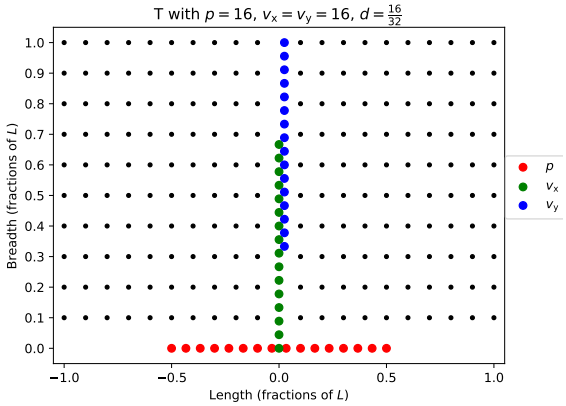

Figure 3.2: T Configuration with $p = v_{\mathbf{x}} = 16,\ d = \frac{16}{32}$

In Figure 3.2, the layout of the T Configuration with $p = v_{\mathrm{x}} = 16,\ d = \frac{16}{32}$ is shown. Unlike in Figure 3.1, the line segment occupied by v_{y} sensors overlaps with the line segment occupied by the v_{x} to a far lesser extent; the v_{y} segment is moved upwards from the v_{x} segment, however, the total length of the two segments is still equal to 1. Consequently, the distances between any two neighbouring velocity sensors of the same type is smaller. As in Figure 3.1, the v_{y} sensors are moved to the right of the v_{x} sensors, however they are in actuality all located on the vertical line at x = 0.

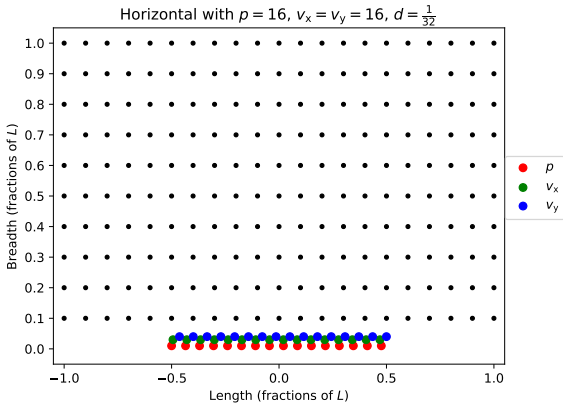

Figure 3.3: Horizontal Configuration with $p = v_{\mathbf{x}} = 16,\ d = \frac{1}{32}$

In Figure 3.3, the layout of the Horizontal Configuration with $p = v_{\mathrm{x}} = 16,\ d = \frac{1}{32}$ is shown. In this figure, it can be seen that the velocity sensors and pressure sensors are all located on a horizontal line at y = 0. Unlike in Figures 3.1 and 3.2, the grid points located in the middle vertical line at x = 0 are not excluded from G. This is because they are located at a distance greater than or equal to 0.1L of the lateral line. The first sensor is a pressure sensor, and the second one is a v_{x} sensor. The distance between these two sensors is equal to a tenth of the distance between any two p sensors, i.e. $\frac{p_{\mathrm{i}}}{10}$. The v_{y} sensors are slightly displaced, towards the right, from the v_{x} sensors, but the two sensor types cover roughly the same line segment. All sensor types are drawn at different y coordinates in order to make them visible, as they overlap to a significant degree, but they are all located along the same horizontal line at y = 0.

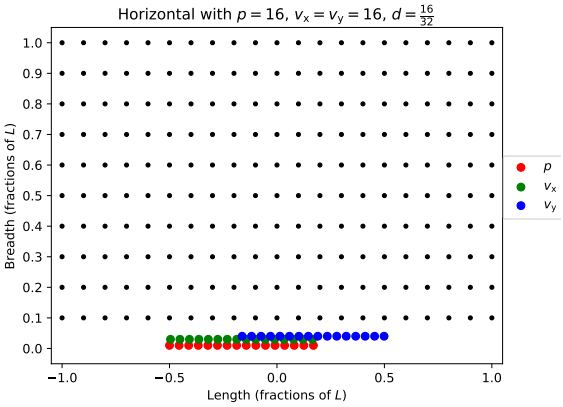

Figure 3.4: Horizontal Configuration with $p = v_{\mathbf{x}} = 16,\ d = \frac{16}{32}$

In Figure 3.4, the layout of the Horizontal Configuration with $p = v_{\mathrm{x}} = 16,\ d = \frac{16}{32}$ is shown. In this figure, unlike in Figure 3.3, the v_{y} sensors overlap to a far lesser degree; there are two intervals along the horizontal line where there are either only p and v_{x} sensors, or where there are only v_{y} sensors. In addition, distances between two neighbouring sensors of the same are smaller, compared to how they were in Figure 3.3, in order for the total length of the lateral line to be 1. As in Figure 3.3, all sensor types are drawn at different y coordinates to make them more distinctive, but are located at y = 0.

3.4 Hyperparameter Optimization

For each configuration used in the experiment, a parameter sweep was performed to find the hidden layer size and activation function with minimal validation error. This was done separately for each component of the output; that is, one parameter sweep was performed for the position error, and one for the orientation error, on the same parameter space. The two components are optimized separately because prior research indicates that they are not necessarily both minimized by the same hyperparameter (Wolf, 2020).

The parameter search space is the set $P = \{(R,\ f) \mid R \in \{400,\ 800,\ 1200,\ 1600\},\ f \in \{\text{ReLU},\ \tanh\}\ \}$, where R is the hidden layer size, and f is the activation function.

This sweep was conducted with a 10-fold cross-validation scheme, splitting the generated data set into 10 folds and, at each iteration, selecting one of the folds to be the validation set and using the remaining 9 folds as the training set. Therefore, 10 different pairs of ELMs were tested for each hidden layer size. This data set is separate from the one used in the main experiment.

3.5 Experiment

The main experiment was conducted by training and testing two neural networks for every sensor configuration on the same randomly generated data set. Per configuration, one ELM was trained to predict the position, and one was trained to predict the orientation. For each configuration and ELM, the combination of hidden layer size and activation function that was identified as having the minimal empirical risk in the parameter sweep stage was used. This means that for each configuration, this optimal combination of hyperparameters may differ between the two ELMs. The T-configurations are tested on the same data set used for the other two, save that data points located directly on the vertical sensor array are excluded.

4 Results

First, example learning curves obtained in the hyperparameter optimization stage are shown.

Afterwards, the mean position and orientation errors of the ELM with different combinations of 32 pressure and velocity sensors are shown. Results are shown separately for horizontal and T configurations.

4.1 Hyperparameters

Figures 4.1 and 4.2 show the validation and training errors for T-configuration $\langle v_x = 5,\ p = 27,\ d = 0.40625\rangle$. The lines represent the errors averaged over 10 folds, and the shaded areas represent the standard deviation of the error.

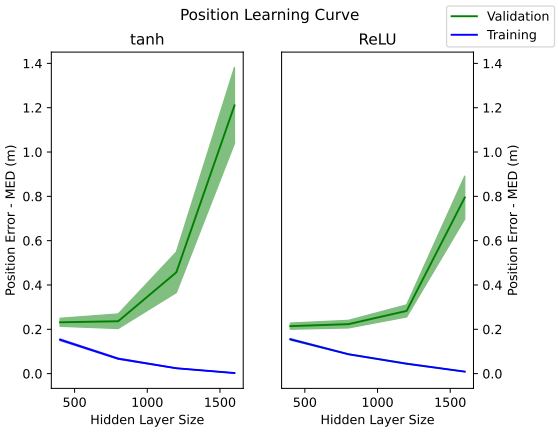

Figure 4.1: Example Position Learning Curve

In Figure 4.1, it can be seen that for both of the two activation functions, the minimal validation error is achieved with a hidden layer size $R = 400$. The validation error is smaller with ReLU than with tanh, and the standard deviation is also lower, so therefore in the final experiment, for the example configuration, the ELM used to predict the position had a hidden layer size $R = 400$ and used ReLU as its activation function.

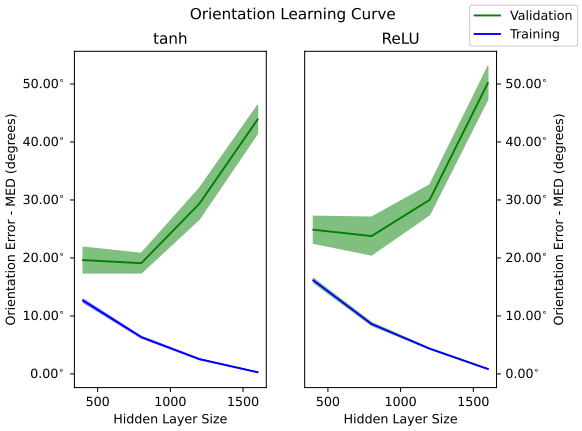

Figure 4.2: Example Orientation Learning Curve

In Figure 4.2, the minimal orientation error is smaller when using tanh as the activation function. This minimal error is achieved, in both cases, when the hidden layer size R is equal to 400. The ELM used to predict the orientation therefore used a hidden layer size $R = 400$ and an activation function tanh; for the position error, the ELM uses the ReLU activation function, because, while the minimum mean error is equal in both cases, ReLU has a smaller standard deviation. In the case that the two average errors are equal between two hyperparameter pairs, the one with the smaller coefficient of variance is picked first.

As it can be seen in both figures, the standard deviations for the validation errors are rather high, relative to the median. This is more pronounced for ELMs with many hidden neurons, which also have a high training error.

The hyperparameters used for each configuration are listed in Appendix A.

4.2 Main Experiment Results

Position and orientation errors for T and horizontal configurations are shown.

Afterwards, violin plots of the errors are shown, for assessing the spread of the error and comparing it between position and orientation.

The vertical and horizontal axes in Figures 4.3 and 4.4 indicate the displacement and the number of velocity sensors $v_x = v_y$, respectively. Each coloured point in the plot corresponds to a sensor configuration corresponding to the vertical displacement and the number of velocity sensors at that point. The colour of each point indicates the mean error obtained for the configuration in the cross-validation phase. The colour bar below the plots describe the relationship between the colour of a point and the error obtained at the respective point; red, darker points have higher error, whereas lighter points have a smaller error. In addition, in each plot, the points are distributed into rows and columns. The bottom-most rows have very low displacement between the v_x and the v_y sensors; the lowest row corresponds to configurations wherein the v_x and v_y sensors are nearly colocational. The upper rows have increasingly higher displacement.

In each figure, the position error is given in the left plot, and the orientation in the right plot. The position error is measured in fractions of L. In addition, in each figure, the extrema of the colour bars have been rounded to the closest number with no more than 2 digits after the decimal point, in order to enhance readability.

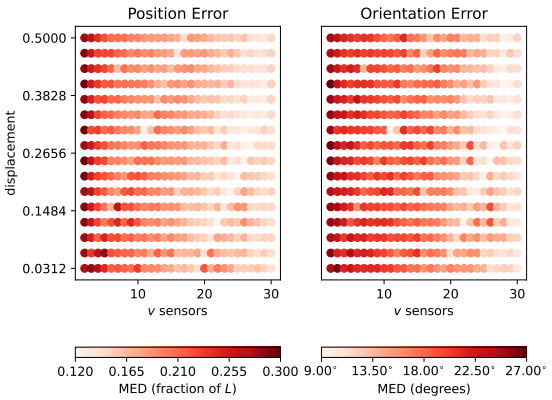

Figure 4.3: Errors for T configurations

In Figure 4.3, it can be seen that the position error is minimal in a diagonal line starting at the bottom-most row with $v = 19$, protruding upwards to the right up to the top row with $v \in [25, 30]$. The position error is maximal when there are few velocity sensors, and it decreases as velocity sensors are added. In addition, the error appears to increase with the displacement. This is also true for the orientation error, save that the orientation error decreases more slowly than the position er-

ror. The same region of minimal error is observed for the orientation error as for the position error. This is likely because as both the number of velocity sensors and the displacement increases, the distance between two velocity sensors (of the same type) decreases, leading to greater coverage of the line segment by the velocity sensors, thereby lessening the gaps in the velocity profile.

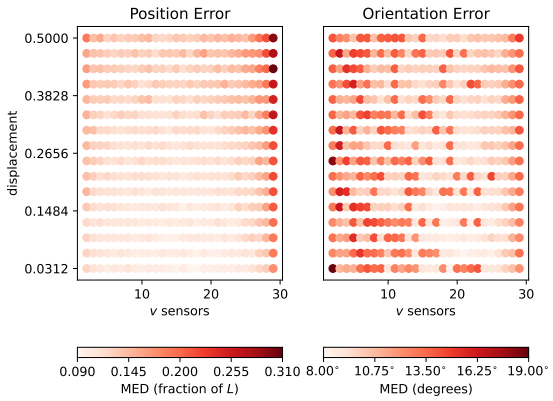

Figure 4.4: Errors for horizontal configurations

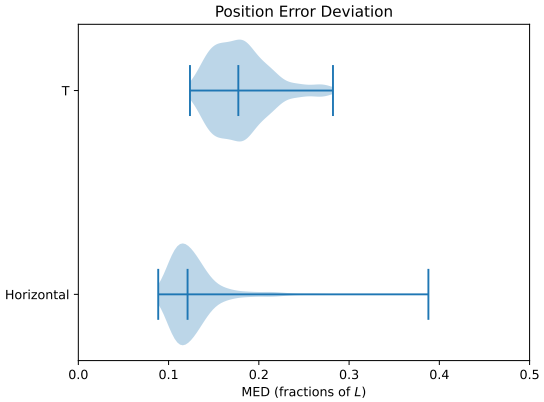

Figure 4.5: Position Violin Plot

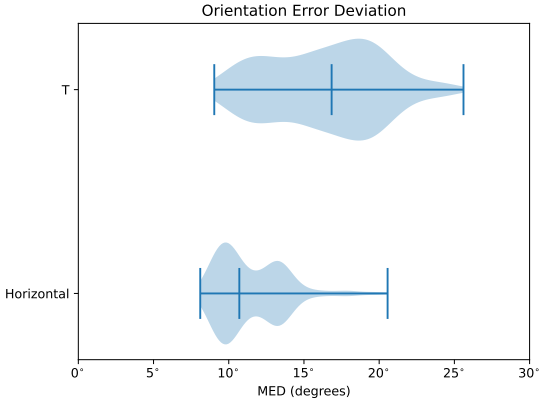

Figure 4.6: Orientation Violin Plot

For the horizontal configurations, the very last data point along the x-axis (corresponding to $v = 30$) was removed, as very high errors, close to 0.9L for the position, were obtained. They were removed from both the position and orientation error plot.

In Figure 4.4, it can be seen that the position error has a mostly small value, close to the minimum, except for when v is very close to 30. No region in particular seems to have minimal error, but one noticeable trend is the increase of the position error with the displacement. For the orientation error, the errors are highest when v is small, and there appears to be a region of minimal orientation error in the right half of the plot.

In Figures 4.5 and 4.6, the widths of the coloured areas represent the density of the data; the wider the area, the more frequently an error value given by the x-axis appears in the distribution of errors. The left-most and right-most line segments show the minima and maxima of the errors. The line segment in between them marks the median. In each figure, the errors from the T-configurations are plotted at the top, and the errors from the horizontal configurations at the bottom.

In both figures, it can be seen that the median for the horizontal errors is lower than for T error; in fact, the median for the T-configuration errors appears to be higher than the vast majority of the horizontal configuration errors. In addition, the violin plots for the horizontal configuration errors

are more squished, indicating that the values are packed around the median. There is one outlier in the position error for the horizontal error, with a value close to 0.5. This might be due to the extreme learning machine being tested on corners of the grid that it has no training data from. Lastly, excluding this outlier, the position error appears to have less spread than the orientation error.

5 Discussion

The position error is smaller in the horizontal configurations than it is in the T-configurations. Furthermore, it appears that the error does not decrease substantially if there are many pressure sensors compared to velocity sensors. For parties interested in making lateral lines with a smaller budget or with limited resources, this can be advantageous, because it implies one can replace velocity sensors, which tend to be more expensive, with pressure sensors, which are cheaper and easier to build, and still achieve high position accuracy. From a technical point of view, the results obtained with the horizontal configurations are interesting because they imply that the pressure profile from the horizontal lateral line has enough information such that the removal of the bidimensional velocity sensors does not impact accuracy too much. Future research could explore the usage of lateral lines utilizing solely pressure sensitive-arrays with no velocity sensors, as it could be the case that having a few velocity sensors improves accuracy, compared to having no velocity sensors at all.

Of note is that the orientation errors don't show the same behaviour. In order for the orientation to be accurately predicted, one needs more velocity sensors than for the position. This could imply that the orientation is in general harder to detect than the position in the localization problem, using pressure sensors. The velocity profile appears to encode important information about the orientation.

The T-configurations performed worse compared to the horizontal configurations. This could be due the two separate sensors arrays picking up two spatially distinct profiles; however, the T-configurations may perform better when the moving object is close to one of the sensor arrays, but farther from the other; it is one way of dealing with the spatial broadening problem. The best T-configurations, for the position component, are those where there are equal or more velocity sensors compared to the number of pressure sensors. For the orientation, the same pattern was observed as in the horizontal configurations. This suggests that the velocity sensors do encode important portions of the orientation information.

6 Conclusion

In short, it seems that pressure sensors could be used to replace some of the velocity sensors in a lateral line. This can be beneficial when velocity sensors are more difficult to acquire or construct. For detecting the position, horizontal configurations perform best, and require few velocity sensors. However, detecting the orientation with higher accuracy requires the addition of velocity sensors to a lateral line. It is therefore important to have as many velocity sensors as possible, and to only fall back on using pressure sensors if the accuracy is already high enough.

References

Bleckmann, H., & Zelick, R. (2009). Lateral line system of fish. *Integrative zoology*, *4*(1), 13–25.

Bot, D. M., Wolf, B. J., & van Netten, S. M. (2021). The quadrature method: A novel dipole localisation algorithm for artificial lateral lines compared to state of the art. *Sensors*, *21*(13), 4558.

Boulogne, L. H., Wolf, B. J., Wiering, M. A., & van Netten, S. M. (2017). Performance of neural networks for localizing moving objects with an artificial lateral line. *Bioinspiration & biomimetics*, *12*(5), 056009.

Curcic-Blake, B., & van Netten, S. M. (2006). Source location encoding in the fish lateral line canal. *Journal of Experimental Biology*, *209*(8), 1548–1559.

Franosch, J.-M. P., Sichert, A. B., Suttner, M. D., & Hemmen, J. (2005). Estimating position and velocity of a submerged moving object by the clawed frog xenopus and by fish—a cybernetic approach. *Biological cybernetics*, *93*(4), 231–238.

Huang, G.-B., Zhu, Q.-Y., & Siew, C.-K. (2006). Extreme learning machine: theory and applications. *Neurocomputing*, *70*(1-3), 489–501.

Lamb, H. (1932). Hydrodynamics, cambridge univ. *Press,*, 134–139.

Netten, S. M. v., & McHenry, M. J. (2013). The biophysics of the fish lateral line. In *The lateral line system* (pp. 99–119). Springer.

Venturelli, R., Akanyeti, O., Visentin, F., Ježov, J., Chambers, L. D., Toming, G., ... Fiorini, P. (2012). Hydrodynamic pressure sensing with an artificial lateral line in steady and unsteady flows. *Bioinspiration & biomimetics*, *7*(3), 036004.

Wolf, B. J. (2020). Hydrodynamic imaging with artificial intelligence: detecting submerged objects at a distance using a 2d-sensitive flow sensor array and neural networks.

Wolf, B. J., Morton, J. A., MacPherson, W. N., & Van Netten, S. M. (2018). Bio-inspired all-optical artificial neuromast for 2d flow sensing. *Bioinspiration & biomimetics*, *13*(2), 026013.

Wolf, B. J., & van Netten, S. M. (2019). Training submerged source detection for a 2d fluid flow sensor array with extreme learning machines. In *Eleventh international conference on machine vision (icmv 2018)* (Vol. 11041, pp. 588–595).

A Appendix

A.1 T Configurations Position Hyperparameters

In the tables given below, the first column gives the number of velocity sensors v_x. The number of pressure sensors is equal to 32 - v_x.

Velocity v_x Sensors	Displacement	Layer Size	Activation	Validation Error	SD
2	0.031	400	tanh	0.277	0.018
2	0.062	400	ReLU	0.273	0.016
2	0.094	400	ReLU	0.276	0.015
2	0.125	400	ReLU	0.272	0.023
2	0.156	400	ReLU	0.276	0.010
2	0.188	400	tanh	0.275	0.025
2	0.219	400	ReLU	0.273	0.024
2	0.250	400	tanh	0.279	0.024
2	0.281	400	ReLU	0.267	0.014
2	0.312	400	tanh	0.278	0.021
2	0.344	400	ReLU	0.277	0.017
2	0.375	400	tanh	0.280	0.025
2	0.406	400	tanh	0.282	0.022
2	0.438	400	tanh	0.274	0.017
2	0.469	400	ReLU	0.275	0.016
2	0.500	400	ReLU	0.281	0.013
3	0.031	400	ReLU	0.238	0.015
3	0.062	400	ReLU	0.252	0.017
3	0.094	400	ReLU	0.236	0.013
3	0.125	400	ReLU	0.245	0.014
3	0.156	400	ReLU	0.239	0.010
3	0.188	400	ReLU	0.239	0.016
3	0.219	400	ReLU	0.244	0.016
3	0.250	400	tanh	0.229	0.014
3	0.281	400	ReLU	0.238	0.018
3	0.312	400	ReLU	0.239	0.015
3	0.344	400	tanh	0.255	0.023
3	0.375	400	ReLU	0.237	0.015
3	0.406	400	ReLU	0.247	0.024
3	0.438	400	ReLU	0.258	0.022
3	0.469	400	ReLU	0.239	0.011
3	0.500	400	tanh	0.232	0.009
4	0.031	800	ReLU	0.215	0.013
4	0.062	800	ReLU	0.219	0.018
4	0.094	800	ReLU	0.213	0.013
4	0.125	800	ReLU	0.222	0.015
4	0.156	800	ReLU	0.221	0.019
4	0.188	800	ReLU	0.223	0.011
4	0.219	800	ReLU	0.227	0.020
4	0.250	800	ReLU	0.228	0.010

4	0.281	800	ReLU	0.219	0.018
4	0.312	800	ReLU	0.220	0.017
4	0.344	400	ReLU	0.227	0.015
4	0.375	800	ReLU	0.222	0.016
4	0.406	800	ReLU	0.232	0.022
4	0.438	400	ReLU	0.223	0.009
4	0.469	400	ReLU	0.235	0.018
4	0.500	400	ReLU	0.233	0.015
5	0.031	800	ReLU	0.197	0.010
5	0.062	800	tanh	0.200	0.021
5	0.094	800	ReLU	0.199	0.014
5	0.125	800	ReLU	0.210	0.016
5	0.156	800	ReLU	0.211	0.011
5	0.188	800	ReLU	0.208	0.011
5	0.219	800	ReLU	0.216	0.019
5	0.250	400	ReLU	0.210	0.011
5	0.281	800	ReLU	0.204	0.019
5	0.312	800	ReLU	0.213	0.013
5	0.344	800	ReLU	0.218	0.016
5	0.375	400	ReLU	0.212	0.010
5	0.406	400	ReLU	0.219	0.016
5	0.438	400	ReLU	0.214	0.014
5	0.469	400	ReLU	0.226	0.010
5	0.500	400	ReLU	0.211	0.014
6	0.031	800	ReLU	0.204	0.019
6	0.062	800	ReLU	0.193	0.016
6	0.094	800	ReLU	0.197	0.010
6	0.125	800	ReLU	0.200	0.015
6	0.156	800	ReLU	0.208	0.012
6	0.188	800	ReLU	0.214	0.019
6	0.219	800	ReLU	0.209	0.013
6	0.250	800	ReLU	0.204	0.013
6	0.281	800	ReLU	0.213	0.015
6	0.312	400	ReLU	0.207	0.009
6	0.344	800	ReLU	0.215	0.020
6	0.375	800	ReLU	0.216	0.012
6	0.406	400	ReLU	0.222	0.013
6	0.438	800	ReLU	0.212	0.018
6	0.469	400	ReLU	0.216	0.010
6	0.500	400	ReLU	0.211	0.014
7	0.031	800	ReLU	0.197	0.012
7	0.062	800	ReLU	0.194	0.016
7	0.094	800	ReLU	0.195	0.016
7	0.125	800	tanh	0.199	0.020
7	0.156	800	tanh	0.194	0.022
7	0.188	800	ReLU	0.198	0.009
7	0.219	800	ReLU	0.199	0.013

7	0.250	800	ReLU	0.165	0.010
7	0.281	800	ReLU	0.204	0.012
7	0.312	800	ReLU	0.205	0.013
7	0.344	800	ReLU	0.208	0.016
7	0.375	800	ReLU	0.203	0.013
7	0.406	800	ReLU	0.202	0.013
7	0.438	800	ReLU	0.212	0.022
7	0.469	800	ReLU	0.213	0.021
7	0.500	800	ReLU	0.208	0.014
8	0.031	800	ReLU	0.189	0.012
8	0.062	800	ReLU	0.183	0.009
8	0.094	800	ReLU	0.191	0.011
8	0.125	800	ReLU	0.196	0.016
8	0.156	800	ReLU	0.198	0.018
8	0.188	800	ReLU	0.187	0.013
8	0.219	800	ReLU	0.189	0.016
8	0.250	800	ReLU	0.201	0.016
8	0.281	800	ReLU	0.195	0.016
8	0.312	800	ReLU	0.212	0.013
8	0.344	800	ReLU	0.196	0.014
8	0.375	800	ReLU	0.204	0.020
8	0.406	800	ReLU	0.203	0.010
8	0.438	800	ReLU	0.210	0.020
8	0.469	800	ReLU	0.197	0.009
8	0.500	800	ReLU	0.199	0.018
9	0.031	800	ReLU	0.187	0.008
9	0.062	800	ReLU	0.183	0.015
9	0.094	800	ReLU	0.181	0.013
9	0.125	800	tanh	0.186	0.016
9	0.156	800	ReLU	0.193	0.011
9	0.188	800	ReLU	0.190	0.009
9	0.219	800	ReLU	0.187	0.015
9	0.250	800	ReLU	0.191	0.020
9	0.281	800	ReLU	0.195	0.015
9	0.312	800	ReLU	0.198	0.019
9	0.344	800	ReLU	0.198	0.011
9	0.375	800	ReLU	0.204	0.017
9	0.406	400	ReLU	0.205	0.009
9	0.438	800	ReLU	0.206	0.014
9	0.469	800	ReLU	0.194	0.012
9	0.500	800	ReLU	0.198	0.014
10	0.031	800	tanh	0.173	0.011
10	0.062	800	ReLU	0.180	0.012
10	0.094	800	ReLU	0.189	0.010
10	0.125	800	ReLU	0.182	0.013
10	0.156	800	ReLU	0.189	0.012
10	0.188	800	ReLU	0.193	0.010

10	0.219	800	ReLU	0.190	0.015
10	0.250	800	ReLU	0.187	0.013
10	0.281	800	ReLU	0.191	0.013
10	0.312	800	ReLU	0.197	0.014
10	0.344	800	ReLU	0.195	0.014
10	0.375	800	ReLU	0.199	0.014
10	0.406	400	ReLU	0.205	0.004
10	0.438	400	ReLU	0.215	0.015
10	0.469	400	ReLU	0.196	0.012
10	0.500	400	ReLU	0.202	0.013
11	0.031	800	ReLU	0.178	0.008
11	0.062	800	ReLU	0.174	0.008
11	0.094	800	ReLU	0.169	0.010
11	0.125	800	ReLU	0.174	0.015
11	0.156	800	ReLU	0.183	0.009
11	0.188	800	ReLU	0.177	0.015
11	0.219	800	ReLU	0.185	0.012
11	0.250	400	ReLU	0.177	0.008
11	0.281	800	ReLU	0.191	0.017
11	0.312	800	ReLU	0.181	0.014
11	0.344	800	ReLU	0.193	0.012
11	0.375	800	ReLU	0.186	0.018
11	0.406	400	ReLU	0.198	0.009
11	0.438	800	ReLU	0.200	0.019
11	0.469	400	ReLU	0.195	0.011
11	0.500	800	ReLU	0.162	0.010
12	0.031	400	ReLU	0.187	0.006
12	0.062	800	ReLU	0.184	0.011
12	0.094	800	ReLU	0.178	0.010
12	0.125	800	ReLU	0.179	0.010
12	0.156	800	ReLU	0.183	0.010
12	0.188	800	ReLU	0.181	0.012
12	0.219	800	ReLU	0.180	0.011
12	0.250	800	ReLU	0.194	0.017
12	0.281	800	ReLU	0.185	0.011
12	0.312	800	ReLU	0.191	0.008
12	0.344	800	ReLU	0.190	0.016
12	0.375	800	ReLU	0.184	0.012
12	0.406	800	ReLU	0.187	0.010
12	0.438	800	ReLU	0.190	0.013
12	0.469	800	ReLU	0.192	0.013
12	0.500	400	ReLU	0.190	0.009
13	0.031	800	ReLU	0.162	0.009
13	0.062	800	tanh	0.174	0.014
13	0.094	800	ReLU	0.183	0.013
13	0.125	800	ReLU	0.181	0.014
13	0.156	800	ReLU	0.171	0.010

13	0.188	800	ReLU	0.172	0.015
13	0.219	800	ReLU	0.171	0.011
13	0.250	800	ReLU	0.174	0.008
13	0.281	400	ReLU	0.184	0.010
13	0.312	800	ReLU	0.183	0.012
13	0.344	800	ReLU	0.185	0.013
13	0.375	800	ReLU	0.185	0.017
13	0.406	800	ReLU	0.188	0.013
13	0.438	800	ReLU	0.184	0.013
13	0.469	800	ReLU	0.188	0.017
13	0.500	800	ReLU	0.186	0.009
14	0.031	800	ReLU	0.169	0.011
14	0.062	800	ReLU	0.173	0.013
14	0.094	800	ReLU	0.170	0.013
14	0.125	800	ReLU	0.178	0.014
14	0.156	800	ReLU	0.172	0.009
14	0.188	800	ReLU	0.183	0.015
14	0.219	800	ReLU	0.178	0.010
14	0.250	800	ReLU	0.187	0.015
14	0.281	800	ReLU	0.184	0.016
14	0.312	400	ReLU	0.182	0.010
14	0.344	800	ReLU	0.187	0.012
14	0.375	800	ReLU	0.182	0.010
14	0.406	800	ReLU	0.187	0.013
14	0.438	400	ReLU	0.190	0.009
14	0.469	400	ReLU	0.190	0.010
14	0.500	800	ReLU	0.188	0.011
15	0.031	800	ReLU	0.162	0.009
15	0.062	800	tanh	0.161	0.008
15	0.094	800	ReLU	0.160	0.007
15	0.125	800	ReLU	0.159	0.010
15	0.156	800	ReLU	0.177	0.012
15	0.188	800	ReLU	0.174	0.010
15	0.219	800	ReLU	0.179	0.012
15	0.250	800	ReLU	0.155	0.013
15	0.281	800	ReLU	0.186	0.012
15	0.312	800	ReLU	0.173	0.012
15	0.344	800	ReLU	0.174	0.015
15	0.375	800	ReLU	0.179	0.015
15	0.406	800	ReLU	0.177	0.016
15	0.438	400	ReLU	0.188	0.006
15	0.469	400	ReLU	0.189	0.006
15	0.500	400	ReLU	0.181	0.010
16	0.031	800	ReLU	0.149	0.013
16	0.062	800	ReLU	0.160	0.010
16	0.094	800	ReLU	0.165	0.008
16	0.125	800	ReLU	0.162	0.009

16	0.156	800	ReLU	0.170	0.013
16	0.188	800	ReLU	0.164	0.009
16	0.219	800	ReLU	0.165	0.008
16	0.250	800	ReLU	0.173	0.012
16	0.281	800	ReLU	0.178	0.010
16	0.312	800	ReLU	0.187	0.011
16	0.344	800	ReLU	0.191	0.011
16	0.375	800	ReLU	0.178	0.011
16	0.406	800	ReLU	0.177	0.010
16	0.438	800	ReLU	0.178	0.009
16	0.469	800	ReLU	0.181	0.011
16	0.500	400	ReLU	0.174	0.007
17	0.031	800	ReLU	0.157	0.011
17	0.062	800	ReLU	0.163	0.009
17	0.094	800	ReLU	0.160	0.013
17	0.125	800	ReLU	0.163	0.008
17	0.156	800	ReLU	0.167	0.011
17	0.188	800	ReLU	0.164	0.012
17	0.219	800	ReLU	0.168	0.014
17	0.250	800	ReLU	0.165	0.008
17	0.281	800	ReLU	0.172	0.012
17	0.312	800	ReLU	0.171	0.008
17	0.344	800	ReLU	0.170	0.008
17	0.375	800	ReLU	0.174	0.010
17	0.406	800	ReLU	0.190	0.013
17	0.438	400	ReLU	0.195	0.010
17	0.469	800	ReLU	0.188	0.016
17	0.500	800	ReLU	0.175	0.016
18	0.031	800	ReLU	0.160	0.010
18	0.062	800	ReLU	0.155	0.008
18	0.094	800	ReLU	0.156	0.007
18	0.125	800	ReLU	0.158	0.010
18	0.156	800	ReLU	0.169	0.013
18	0.188	800	ReLU	0.165	0.014
18	0.219	800	ReLU	0.161	0.013
18	0.250	800	ReLU	0.167	0.012
18	0.281	800	ReLU	0.158	0.007
18	0.312	800	ReLU	0.171	0.011
18	0.344	800	ReLU	0.171	0.011
18	0.375	800	ReLU	0.163	0.014
18	0.406	800	ReLU	0.168	0.010
18	0.438	400	ReLU	0.176	0.010
18	0.469	800	ReLU	0.171	0.011
18	0.500	800	ReLU	0.183	0.009
19	0.031	800	ReLU	0.146	0.009
19	0.062	800	tanh	0.146	0.015
19	0.094	800	ReLU	0.157	0.011

19	0.125	800	ReLU	0.154	0.009
19	0.156	800	ReLU	0.154	0.010
19	0.188	800	ReLU	0.158	0.010
19	0.219	800	ReLU	0.165	0.013
19	0.250	800	ReLU	0.157	0.013
19	0.281	800	ReLU	0.163	0.014
19	0.312	800	ReLU	0.158	0.011
19	0.344	800	ReLU	0.169	0.014
19	0.375	800	ReLU	0.168	0.006
19	0.406	800	ReLU	0.168	0.017
19	0.438	800	ReLU	0.167	0.010
19	0.469	400	ReLU	0.171	0.009
19	0.500	800	ReLU	0.166	0.009
20	0.031	800	tanh	0.147	0.014
20	0.062	800	ReLU	0.144	0.015
20	0.094	800	ReLU	0.153	0.010
20	0.125	800	ReLU	0.153	0.010
20	0.156	800	ReLU	0.154	0.007
20	0.188	800	ReLU	0.159	0.008
20	0.219	800	ReLU	0.162	0.014
20	0.250	800	ReLU	0.159	0.015
20	0.281	400	ReLU	0.165	0.010
20	0.312	800	ReLU	0.155	0.008
20	0.344	800	ReLU	0.167	0.011
20	0.375	800	ReLU	0.165	0.011
20	0.406	800	ReLU	0.165	0.013
20	0.438	400	ReLU	0.169	0.011
20	0.469	800	ReLU	0.168	0.014
20	0.500	400	ReLU	0.174	0.010
21	0.031	800	ReLU	0.151	0.007
21	0.062	800	tanh	0.141	0.010
21	0.094	800	ReLU	0.143	0.007
21	0.125	800	ReLU	0.146	0.009
21	0.156	800	ReLU	0.147	0.008
21	0.188	800	ReLU	0.153	0.008
21	0.219	800	ReLU	0.152	0.009
21	0.250	800	ReLU	0.152	0.015
21	0.281	800	ReLU	0.157	0.010
21	0.312	800	ReLU	0.158	0.010
21	0.344	400	ReLU	0.171	0.007
21	0.375	800	ReLU	0.157	0.009
21	0.406	800	ReLU	0.163	0.012
21	0.438	800	ReLU	0.163	0.009
21	0.469	800	ReLU	0.166	0.011
21	0.500	800	ReLU	0.153	0.010
22	0.031	800	tanh	0.132	0.016
22	0.062	800	ReLU	0.146	0.008

22	0.094	800	ReLU	0.162	0.010
22	0.125	800	tanh	0.173	0.018
22	0.156	400	ReLU	0.160	0.009
22	0.188	800	ReLU	0.139	0.009
22	0.219	800	ReLU	0.145	0.010
22	0.250	800	ReLU	0.156	0.009
22	0.281	800	ReLU	0.151	0.012
22	0.312	800	ReLU	0.155	0.013
22	0.344	800	ReLU	0.153	0.009
22	0.375	800	ReLU	0.153	0.012
22	0.406	400	ReLU	0.163	0.007
22	0.438	800	ReLU	0.163	0.013
22	0.469	800	ReLU	0.159	0.008
22	0.500	400	ReLU	0.168	0.009
23	0.031	800	tanh	0.133	0.014
23	0.062	800	ReLU	0.140	0.012
23	0.094	800	ReLU	0.137	0.009
23	0.125	800	ReLU	0.137	0.009
23	0.156	800	ReLU	0.140	0.010
23	0.188	800	ReLU	0.148	0.005
23	0.219	800	ReLU	0.162	0.011
23	0.250	800	ReLU	0.149	0.011
23	0.281	800	ReLU	0.167	0.013
23	0.312	400	ReLU	0.156	0.007
23	0.344	800	ReLU	0.149	0.007
23	0.375	800	ReLU	0.151	0.012
23	0.406	800	ReLU	0.153	0.013
23	0.438	800	ReLU	0.160	0.011
23	0.469	800	ReLU	0.162	0.017
23	0.500	800	ReLU	0.159	0.008
24	0.031	800	tanh	0.132	0.017
24	0.062	800	ReLU	0.141	0.011
24	0.094	800	ReLU	0.140	0.006
24	0.125	800	ReLU	0.138	0.006
24	0.156	800	ReLU	0.142	0.010
24	0.188	800	ReLU	0.146	0.011
24	0.219	800	ReLU	0.151	0.008
24	0.250	800	ReLU	0.147	0.011
24	0.281	800	ReLU	0.147	0.010
24	0.312	800	ReLU	0.150	0.013
24	0.344	800	ReLU	0.153	0.009
24	0.375	800	ReLU	0.159	0.010
24	0.406	400	ReLU	0.178	0.007
24	0.438	800	ReLU	0.180	0.009
24	0.469	800	ReLU	0.168	0.010
24	0.500	400	ReLU	0.163	0.007
25	0.031	800	ReLU	0.130	0.011

25	0.062	800	tanh	0.130	0.012
25	0.094	800	ReLU	0.147	0.010
25	0.125	800	ReLU	0.144	0.009
25	0.156	800	tanh	0.135	0.015
25	0.188	800	ReLU	0.146	0.010
25	0.219	800	ReLU	0.143	0.008
25	0.250	400	ReLU	0.152	0.008
25	0.281	800	ReLU	0.146	0.010
25	0.312	800	ReLU	0.145	0.010
25	0.344	800	ReLU	0.154	0.009
25	0.375	800	ReLU	0.155	0.014
25	0.406	800	ReLU	0.150	0.010
25	0.438	800	ReLU	0.155	0.013
25	0.469	400	ReLU	0.151	0.011
25	0.500	400	ReLU	0.151	0.007
26	0.031	800	tanh	0.136	0.013
26	0.062	800	tanh	0.129	0.017
26	0.094	800	tanh	0.130	0.014
26	0.125	800	tanh	0.134	0.018
26	0.156	800	ReLU	0.136	0.011
26	0.188	800	ReLU	0.143	0.010
26	0.219	800	ReLU	0.142	0.009
26	0.250	800	ReLU	0.149	0.010
26	0.281	800	ReLU	0.147	0.010
26	0.312	800	ReLU	0.148	0.011
26	0.344	800	ReLU	0.158	0.007
26	0.375	800	ReLU	0.147	0.009
26	0.406	800	ReLU	0.151	0.012
26	0.438	800	ReLU	0.155	0.014
26	0.469	800	ReLU	0.153	0.011
26	0.500	400	tanh	0.152	0.011
27	0.031	800	tanh	0.127	0.019
27	0.062	800	tanh	0.133	0.017
27	0.094	800	ReLU	0.128	0.010
27	0.125	800	tanh	0.132	0.021
27	0.156	800	ReLU	0.134	0.006
27	0.188	800	ReLU	0.142	0.013
27	0.219	400	tanh	0.146	0.009
27	0.250	800	ReLU	0.152	0.012
27	0.281	800	ReLU	0.148	0.008
27	0.312	800	ReLU	0.146	0.014
27	0.344	800	ReLU	0.147	0.014
27	0.375	800	ReLU	0.143	0.009
27	0.406	400	ReLU	0.151	0.008
27	0.438	400	ReLU	0.151	0.009
27	0.469	400	tanh	0.150	0.013
27	0.500	800	ReLU	0.147	0.016

28	0.031	800	tanh	0.128	0.013
28	0.062	800	ReLU	0.130	0.014
28	0.094	800	ReLU	0.143	0.010
28	0.125	800	ReLU	0.143	0.008
28	0.156	400	tanh	0.138	0.011
28	0.188	800	ReLU	0.141	0.010
28	0.219	400	tanh	0.140	0.011
28	0.250	400	ReLU	0.152	0.008
28	0.281	800	ReLU	0.141	0.007
28	0.312	400	tanh	0.147	0.016
28	0.344	400	tanh	0.145	0.014
28	0.375	400	tanh	0.145	0.004
28	0.406	400	ReLU	0.146	0.007
28	0.438	400	tanh	0.143	0.010
28	0.469	400	tanh	0.150	0.010
28	0.500	400	tanh	0.146	0.014
29	0.031	800	ReLU	0.147	0.009
29	0.062	400	tanh	0.154	0.017
29	0.094	400	tanh	0.148	0.012
29	0.125	400	tanh	0.147	0.015
29	0.156	400	tanh	0.147	0.010
29	0.188	400	tanh	0.149	0.017
29	0.219	400	tanh	0.146	0.012
29	0.250	400	tanh	0.155	0.011
29	0.281	400	ReLU	0.151	0.007
29	0.312	400	ReLU	0.151	0.005
29	0.344	400	tanh	0.151	0.010
29	0.375	400	tanh	0.149	0.014
29	0.406	400	tanh	0.152	0.017
29	0.438	400	tanh	0.150	0.010
29	0.469	400	tanh	0.150	0.019
29	0.500	400	ReLU	0.151	0.004
30	0.031	400	ReLU	0.170	0.014
30	0.062	400	ReLU	0.172	0.012
30	0.094	400	ReLU	0.171	0.009
30	0.125	400	ReLU	0.173	0.010
30	0.156	400	ReLU	0.168	0.009
30	0.188	400	ReLU	0.171	0.012
30	0.219	400	ReLU	0.171	0.012
30	0.250	400	ReLU	0.173	0.009
30	0.281	400	ReLU	0.168	0.008
30	0.312	400	ReLU	0.172	0.010
30	0.344	400	ReLU	0.171	0.009
30	0.375	400	ReLU	0.168	0.010
30	0.406	400	ReLU	0.168	0.011
30	0.438	400	ReLU	0.168	0.011
30	0.469	400	ReLU	0.171	0.011

30	0.500	400	ReLU	0.167	0.009

A.2 T Configuration Orientation Hyperparameters

Velocity v_x Sensors	Displacement	Layer Size	Activation	Validation Error	SD
2	0.031	400	tanh	24.363	2.119
2	0.062	400	tanh	22.755	1.854
2	0.094	800	tanh	23.759	2.110
2	0.125	400	tanh	24.299	2.021
2	0.156	400	tanh	23.337	1.338
2	0.188	400	tanh	22.782	1.119
2	0.219	400	tanh	24.361	1.467
2	0.250	400	tanh	23.705	1.146
2	0.281	400	tanh	23.201	1.602
2	0.312	400	tanh	24.286	1.550
2	0.344	400	tanh	23.505	1.449
2	0.375	400	tanh	24.567	1.860
2	0.406	400	tanh	23.611	1.420
2	0.438	400	tanh	22.930	1.551
2	0.469	400	tanh	23.695	1.904
2	0.500	400	tanh	23.613	1.181
3	0.031	800	tanh	21.055	1.341
3	0.062	400	tanh	22.246	1.370
3	0.094	400	tanh	20.626	1.451
3	0.125	400	tanh	21.234	1.878
3	0.156	400	tanh	21.428	1.757
3	0.188	400	tanh	21.256	1.691
3	0.219	400	tanh	22.449	1.420
3	0.250	400	tanh	18.866	1.870
3	0.281	400	tanh	21.551	1.652
3	0.312	400	tanh	21.634	1.545
3	0.344	400	tanh	22.481	2.064
3	0.375	400	tanh	21.871	2.321
3	0.406	400	tanh	21.745	1.532
3	0.438	400	tanh	23.554	2.119
3	0.469	400	tanh	21.334	1.918
3	0.500	400	tanh	20.245	1.620
4	0.031	400	tanh	20.029	0.994
4	0.062	400	tanh	20.837	2.081
4	0.094	800	tanh	21.502	1.697
4	0.125	800	tanh	22.381	1.834
4	0.156	400	tanh	19.772	0.994
4	0.188	800	tanh	20.199	3.057
4	0.219	400	tanh	21.091	1.939
4	0.250	800	tanh	20.865	2.314
4	0.281	800	tanh	20.030	1.193

4	0.312	400	tanh	20.313	1.277
4	0.344	400	tanh	20.554	2.194
4	0.375	400	tanh	20.605	2.237
4	0.406	400	tanh	20.124	1.635
4	0.438	400	tanh	19.820	1.830
4	0.469	400	tanh	21.924	1.712
4	0.500	400	tanh	20.152	1.462
5	0.031	800	tanh	19.070	1.361
5	0.062	800	tanh	19.297	2.364
5	0.094	800	tanh	20.447	1.612
5	0.125	400	tanh	19.288	1.406
5	0.156	400	tanh	21.221	1.242
5	0.188	400	tanh	18.816	1.025
5	0.219	800	tanh	18.779	2.219
5	0.250	400	tanh	19.723	1.246
5	0.281	800	tanh	19.517	1.739
5	0.312	400	tanh	19.555	1.535
5	0.344	400	tanh	19.547	1.606
5	0.375	400	tanh	19.671	0.949
5	0.406	400	tanh	19.758	1.017
5	0.438	800	tanh	19.094	1.699
5	0.469	400	tanh	19.773	2.113
5	0.500	400	tanh	18.831	0.998
6	0.031	800	tanh	18.561	1.702
6	0.062	800	tanh	19.212	1.806
6	0.094	400	tanh	19.558	1.416
6	0.125	400	tanh	19.284	1.551
6	0.156	800	tanh	18.314	1.043
6	0.188	400	tanh	20.701	1.804
6	0.219	400	tanh	20.107	1.448
6	0.250	400	tanh	19.163	1.587
6	0.281	400	tanh	18.703	1.608
6	0.312	400	tanh	19.363	1.894
6	0.344	400	tanh	18.791	2.856
6	0.375	800	tanh	19.515	1.430
6	0.406	400	tanh	20.293	2.204
6	0.438	400	tanh	19.999	1.591
6	0.469	400	tanh	19.580	1.879
6	0.500	400	tanh	17.948	1.361
7	0.031	800	tanh	18.452	1.400
7	0.062	800	tanh	17.927	1.436
7	0.094	800	tanh	17.941	1.944
7	0.125	400	tanh	18.692	1.033
7	0.156	800	tanh	19.389	1.237
7	0.188	400	tanh	19.366	1.228
7	0.219	400	tanh	18.442	1.776
7	0.250	400	tanh	12.502	0.959

7	0.281	800	tanh	18.918	2.214
7	0.312	800	tanh	19.527	1.932
7	0.344	400	tanh	18.686	1.306
7	0.375	400	tanh	18.677	1.306
7	0.406	800	tanh	19.881	1.183
7	0.438	400	tanh	18.910	1.251
7	0.469	400	tanh	19.844	1.562
7	0.500	800	tanh	18.218	1.823
8	0.031	800	tanh	17.985	1.168
8	0.062	800	tanh	18.444	1.396
8	0.094	400	tanh	19.208	1.703
8	0.125	800	tanh	18.514	0.898
8	0.156	400	tanh	18.984	1.430
8	0.188	400	tanh	18.678	0.970
8	0.219	800	tanh	18.276	1.601
8	0.250	400	tanh	18.759	1.966
8	0.281	400	tanh	19.288	1.731
8	0.312	400	tanh	20.892	2.420
8	0.344	800	tanh	18.688	2.252
8	0.375	400	tanh	19.252	1.573
8	0.406	400	tanh	18.969	1.950
8	0.438	400	tanh	18.536	1.665
8	0.469	400	tanh	18.815	1.787
8	0.500	400	tanh	18.645	1.096
9	0.031	800	tanh	16.788	2.044
9	0.062	800	tanh	18.842	1.480
9	0.094	800	tanh	17.714	2.151
9	0.125	800	tanh	19.045	0.907
9	0.156	800	tanh	17.527	1.533
9	0.188	800	tanh	18.952	1.724
9	0.219	800	tanh	18.829	2.244
9	0.250	800	tanh	18.166	2.123
9	0.281	800	tanh	18.167	1.406
9	0.312	800	tanh	17.730	1.786
9	0.344	400	tanh	18.368	1.155
9	0.375	400	tanh	19.470	1.854
9	0.406	400	tanh	18.450	1.209
9	0.438	400	tanh	18.681	1.566
9	0.469	400	tanh	18.682	1.565
9	0.500	400	tanh	18.831	1.523
10	0.031	400	tanh	16.642	1.598
10	0.062	400	tanh	18.255	1.533
10	0.094	800	tanh	17.482	1.382
10	0.125	800	tanh	17.635	1.338
10	0.156	800	tanh	17.715	1.169
10	0.188	800	tanh	18.937	1.665
10	0.219	400	tanh	17.731	0.995

10	0.250	800	tanh	17.415	1.951
10	0.281	400	tanh	18.155	1.481
10	0.312	400	tanh	18.845	2.254
10	0.344	800	tanh	18.180	1.842
10	0.375	800	tanh	18.059	1.319
10	0.406	400	tanh	18.985	1.470
10	0.438	800	tanh	19.979	1.770
10	0.469	400	tanh	17.746	1.332
10	0.500	400	tanh	17.522	1.343
11	0.031	800	tanh	16.993	1.359
11	0.062	400	tanh	16.978	1.492
11	0.094	400	tanh	17.295	0.986
11	0.125	800	tanh	16.998	1.836
11	0.156	400	tanh	17.274	1.025
11	0.188	800	tanh	16.975	1.395
11	0.219	800	tanh	17.827	1.307
11	0.250	400	tanh	15.868	1.083
11	0.281	400	tanh	18.969	2.087
11	0.312	800	tanh	17.409	1.337
11	0.344	800	tanh	18.239	1.513
11	0.375	400	tanh	17.275	1.701
11	0.406	800	tanh	18.856	1.761
11	0.438	800	tanh	17.678	2.013
11	0.469	800	tanh	18.384	2.264
11	0.500	400	tanh	12.681	0.988
12	0.031	800	tanh	16.971	1.598
12	0.062	400	tanh	19.664	1.879
12	0.094	400	tanh	17.138	1.089
12	0.125	800	tanh	17.354	1.938
12	0.156	800	tanh	17.232	0.808
12	0.188	400	tanh	17.540	1.827
12	0.219	400	tanh	18.462	1.219
12	0.250	400	tanh	18.465	1.745
12	0.281	400	tanh	17.532	1.216
12	0.312	800	tanh	17.519	1.506
12	0.344	800	tanh	18.094	1.382
12	0.375	400	tanh	17.489	1.104
12	0.406	400	tanh	18.122	1.019
12	0.438	800	tanh	18.266	1.793
12	0.469	400	tanh	17.920	1.476
12	0.500	400	tanh	17.496	1.831
13	0.031	800	tanh	15.993	1.420
13	0.062	800	tanh	15.725	1.505
13	0.094	800	tanh	18.126	2.144
13	0.125	800	tanh	19.259	1.290
13	0.156	400	tanh	16.659	1.356
13	0.188	400	tanh	17.556	1.386

13	0.219	800	tanh	16.122	1.401
13	0.250	800	tanh	17.179	1.175
13	0.281	800	tanh	17.631	1.434
13	0.312	800	tanh	17.073	1.922
13	0.344	800	tanh	17.522	1.430
13	0.375	800	tanh	17.653	1.775
13	0.406	400	tanh	18.087	2.223
13	0.438	800	tanh	17.624	1.171
13	0.469	400	tanh	18.122	1.634
13	0.500	400	tanh	17.539	1.555
14	0.031	800	tanh	17.278	1.369
14	0.062	800	tanh	16.313	1.855
14	0.094	800	tanh	16.736	1.375
14	0.125	400	tanh	16.163	1.279
14	0.156	400	tanh	16.991	1.508
14	0.188	400	tanh	18.636	1.326
14	0.219	800	tanh	15.927	0.718
14	0.250	800	tanh	17.180	1.346
14	0.281	800	tanh	16.712	1.312
14	0.312	400	tanh	17.112	1.796
14	0.344	400	tanh	17.843	1.237
14	0.375	400	tanh	18.067	1.486
14	0.406	400	tanh	17.347	1.951
14	0.438	400	tanh	17.781	1.938
14	0.469	400	tanh	18.235	0.905
14	0.500	400	tanh	16.885	1.531
15	0.031	800	tanh	15.129	1.908
15	0.062	800	tanh	16.132	1.380
15	0.094	400	tanh	14.399	1.499
15	0.125	800	tanh	15.551	1.256
15	0.156	400	tanh	16.365	1.281
15	0.188	800	tanh	15.762	1.362
15	0.219	400	tanh	17.150	0.843
15	0.250	800	tanh	12.798	2.250
15	0.281	400	tanh	16.853	1.359
15	0.312	800	tanh	16.018	1.813
15	0.344	400	tanh	16.508	1.274
15	0.375	400	tanh	16.722	1.730
15	0.406	400	tanh	15.305	0.837
15	0.438	800	tanh	17.402	1.190
15	0.469	800	tanh	17.292	1.678
15	0.500	400	tanh	16.231	1.091
16	0.031	800	tanh	14.165	1.389
16	0.062	400	tanh	15.598	1.521
16	0.094	400	tanh	15.560	2.067
16	0.125	400	tanh	16.384	1.149
16	0.156	400	tanh	15.943	1.062

16	0.188	400	tanh	16.141	1.887
16	0.219	400	tanh	16.179	1.380
16	0.250	800	tanh	16.348	1.278
16	0.281	400	tanh	16.076	1.040
16	0.312	800	tanh	17.335	1.821
16	0.344	400	tanh	18.742	2.321
16	0.375	400	tanh	16.260	1.271
16	0.406	400	tanh	15.275	1.035
16	0.438	400	tanh	16.956	1.441
16	0.469	400	tanh	17.145	1.544
16	0.500	400	tanh	15.980	1.131
17	0.031	800	tanh	14.537	1.146
17	0.062	400	tanh	15.952	1.145
17	0.094	800	tanh	14.096	1.409
17	0.125	400	tanh	15.883	1.761
17	0.156	400	tanh	15.436	1.863
17	0.188	400	tanh	15.716	1.002
17	0.219	800	tanh	15.244	1.486
17	0.250	400	tanh	16.173	1.438
17	0.281	800	tanh	16.008	2.564
17	0.312	400	tanh	16.334	1.800
17	0.344	400	tanh	15.730	1.100
17	0.375	400	tanh	16.052	1.555
17	0.406	400	tanh	18.046	0.805
17	0.438	800	tanh	19.004	1.219
17	0.469	400	tanh	17.136	1.160
17	0.500	400	tanh	15.907	0.771
18	0.031	800	tanh	15.073	1.351
18	0.062	800	tanh	14.580	1.601
18	0.094	800	tanh	14.864	0.922
18	0.125	400	tanh	14.231	0.741
18	0.156	800	tanh	16.830	1.284
18	0.188	400	tanh	14.360	1.670
18	0.219	400	tanh	14.946	0.923
18	0.250	400	tanh	16.118	1.408
18	0.281	400	tanh	15.040	1.388
18	0.312	400	tanh	16.005	1.212
18	0.344	400	tanh	15.066	1.077
18	0.375	400	tanh	15.251	1.859
18	0.406	400	tanh	15.645	0.983
18	0.438	400	tanh	16.193	1.750
18	0.469	800	tanh	16.307	1.478
18	0.500	400	tanh	16.224	1.606
19	0.031	800	tanh	13.710	1.946
19	0.062	800	tanh	12.608	0.946
19	0.094	400	tanh	13.781	0.982
19	0.125	400	tanh	14.170	0.983

19	0.156	400	tanh	14.719	1.147
19	0.188	400	tanh	14.877	1.066
19	0.219	400	tanh	13.779	0.754
19	0.250	800	tanh	13.520	1.574
19	0.281	400	tanh	14.300	0.855
19	0.312	800	tanh	15.517	1.624
19	0.344	400	tanh	14.995	1.430
19	0.375	400	tanh	15.006	1.299
19	0.406	400	tanh	16.713	0.694
19	0.438	400	tanh	15.724	0.639
19	0.469	400	tanh	16.140	1.791
19	0.500	400	tanh	14.931	0.691
20	0.031	400	tanh	13.161	1.658
20	0.062	800	tanh	12.448	1.453
20	0.094	800	tanh	12.116	0.745
20	0.125	400	tanh	14.855	1.547
20	0.156	400	tanh	13.503	1.418
20	0.188	800	tanh	12.879	1.482
20	0.219	400	tanh	14.355	1.819
20	0.250	800	tanh	14.503	0.970
20	0.281	400	tanh	14.532	1.457
20	0.312	400	tanh	14.309	1.419
20	0.344	400	tanh	14.900	0.909
20	0.375	400	tanh	16.432	1.015
20	0.406	400	tanh	15.183	0.698
20	0.438	400	tanh	15.374	1.416
20	0.469	400	tanh	14.366	1.533
20	0.500	400	tanh	15.692	1.249
21	0.031	400	tanh	14.257	1.760
21	0.062	400	tanh	11.957	1.310
21	0.094	400	tanh	12.423	0.939
21	0.125	800	tanh	12.474	1.452
21	0.156	400	tanh	13.161	0.883
21	0.188	800	tanh	12.959	1.426
21	0.219	400	tanh	12.648	1.343
21	0.250	800	tanh	12.757	1.591
21	0.281	400	tanh	14.587	1.108
21	0.312	400	tanh	13.618	1.497
21	0.344	400	tanh	14.888	1.378
21	0.375	400	tanh	14.120	1.143
21	0.406	400	tanh	15.088	1.127
21	0.438	400	tanh	15.165	1.111
21	0.469	400	tanh	15.272	1.398
21	0.500	800	tanh	12.300	1.427
22	0.031	400	tanh	11.357	0.900
22	0.062	400	tanh	12.568	1.680
22	0.094	400	tanh	15.397	0.670

22	0.125	800	tanh	16.755	2.715
22	0.156	400	tanh	13.586	1.227
22	0.188	400	tanh	12.594	1.182
22	0.219	800	tanh	12.200	1.695
22	0.250	400	tanh	13.500	1.123
22	0.281	400	tanh	12.938	1.242
22	0.312	400	tanh	12.958	0.950
22	0.344	400	tanh	12.988	0.733
22	0.375	400	tanh	13.363	1.125
22	0.406	400	tanh	13.886	1.096
22	0.438	400	tanh	14.572	1.387
22	0.469	800	tanh	15.510	2.054
22	0.500	400	tanh	14.593	1.660
23	0.031	800	tanh	10.458	1.268
23	0.062	800	tanh	10.656	1.387
23	0.094	400	tanh	10.556	0.577
23	0.125	800	tanh	10.778	1.199
23	0.156	800	tanh	11.714	1.277
23	0.188	800	tanh	12.788	1.061
23	0.219	800	tanh	14.859	1.197
23	0.250	800	tanh	12.206	1.744
23	0.281	800	tanh	14.629	0.994
23	0.312	400	tanh	13.543	1.143
23	0.344	400	tanh	12.244	0.925
23	0.375	400	tanh	12.889	1.223
23	0.406	400	tanh	12.258	1.529
23	0.438	400	tanh	13.798	0.999
23	0.469	400	tanh	13.488	1.239
23	0.500	400	tanh	12.640	0.795
24	0.031	800	tanh	10.623	1.375
24	0.062	800	tanh	12.011	1.295
24	0.094	800	tanh	11.048	0.881
24	0.125	800	tanh	11.448	1.024
24	0.156	400	tanh	10.834	1.190
24	0.188	400	tanh	12.489	0.863
24	0.219	400	tanh	12.754	1.259
24	0.250	800	tanh	12.065	2.185
24	0.281	800	tanh	11.789	1.344
24	0.312	400	tanh	11.849	1.085
24	0.344	400	tanh	12.565	0.938
24	0.375	400	tanh	13.878	1.623
24	0.406	400	tanh	16.786	1.504
24	0.438	400	tanh	18.098	1.542
24	0.469	400	tanh	15.271	0.894
24	0.500	800	tanh	13.322	1.255
25	0.031	800	tanh	9.490	1.399
25	0.062	800	tanh	9.446	0.900

25	0.094	800	tanh	11.975	1.213
25	0.125	400	tanh	12.436	0.985
25	0.156	400	tanh	10.488	0.761
25	0.188	400	tanh	11.909	1.032
25	0.219	800	tanh	10.796	1.067
25	0.250	400	tanh	11.809	1.262
25	0.281	800	tanh	10.670	1.246
25	0.312	400	tanh	11.604	1.096
25	0.344	800	tanh	12.450	2.122
25	0.375	400	tanh	12.234	1.169
25	0.406	400	tanh	11.616	1.020
25	0.438	400	tanh	13.165	1.354
25	0.469	800	tanh	12.243	1.199
25	0.500	400	tanh	12.319	1.011
26	0.031	400	tanh	11.271	0.821
26	0.062	400	tanh	9.783	0.756
26	0.094	800	tanh	9.150	1.104
26	0.125	800	tanh	10.069	1.103
26	0.156	400	tanh	10.775	0.815
26	0.188	400	tanh	11.242	0.744
26	0.219	800	tanh	10.408	0.942
26	0.250	400	tanh	11.818	1.046
26	0.281	400	tanh	11.103	1.241
26	0.312	400	tanh	11.992	1.355
26	0.344	400	tanh	13.536	0.547
26	0.375	400	tanh	11.803	1.138
26	0.406	800	tanh	11.221	1.366
26	0.438	400	tanh	12.773	0.995
26	0.469	400	tanh	11.859	0.888
26	0.500	800	tanh	12.045	1.855
27	0.031	800	tanh	9.173	1.435
27	0.062	800	tanh	10.586	1.285
27	0.094	800	tanh	9.128	1.323
27	0.125	800	tanh	9.542	1.442
27	0.156	800	tanh	9.846	1.305
27	0.188	800	tanh	9.850	1.242
27	0.219	400	tanh	12.247	1.408
27	0.250	800	tanh	12.145	1.393
27	0.281	400	tanh	12.399	1.244
27	0.312	800	tanh	10.839	1.363
27	0.344	400	tanh	10.930	0.912
27	0.375	400	tanh	11.075	1.181
27	0.406	800	tanh	11.475	1.239
27	0.438	800	tanh	12.824	1.666
27	0.469	400	tanh	11.667	0.936
27	0.500	800	tanh	11.577	1.688
28	0.031	800	tanh	9.666	0.995

28	0.062	800	tanh	9.900	1.299
28	0.094	800	tanh	11.608	0.935
28	0.125	400	tanh	11.885	1.138
28	0.156	800	tanh	10.407	1.555
28	0.188	800	tanh	10.447	1.588
28	0.219	400	tanh	10.778	0.897
28	0.250	800	tanh	12.575	1.563
28	0.281	800	tanh	10.381	1.621
28	0.312	400	tanh	11.549	0.802
28	0.344	400	tanh	12.734	1.584
28	0.375	400	tanh	11.440	0.718
28	0.406	400	tanh	11.818	0.957
28	0.438	400	tanh	12.319	1.312
28	0.469	400	tanh	11.847	1.469
28	0.500	400	tanh	11.825	1.354
29	0.031	400	tanh	11.874	1.072
29	0.062	400	tanh	11.237	1.236
29	0.094	400	tanh	11.174	0.936
29	0.125	400	tanh	11.720	0.898
29	0.156	400	tanh	11.296	1.062
29	0.188	400	tanh	11.664	0.704
29	0.219	400	tanh	11.769	1.039
29	0.250	400	tanh	13.951	1.091
29	0.281	400	tanh	12.242	0.780
29	0.312	400	tanh	11.710	0.871
29	0.344	400	tanh	12.151	1.772
29	0.375	400	tanh	12.184	1.039
29	0.406	400	tanh	12.476	1.233
29	0.438	400	tanh	13.227	0.964
29	0.469	400	tanh	12.458	0.993
29	0.500	400	tanh	12.436	1.349
30	0.031	400	tanh	12.619	1.130
30	0.062	400	tanh	13.030	1.826
30	0.094	400	tanh	12.838	0.671
30	0.125	400	tanh	13.423	1.009
30	0.156	400	tanh	12.710	1.335
30	0.188	400	tanh	13.019	1.313
30	0.219	400	tanh	13.210	1.249
30	0.250	400	tanh	15.033	1.232
30	0.281	400	tanh	13.525	1.373
30	0.312	400	tanh	14.460	0.942
30	0.344	400	tanh	13.712	1.194
30	0.375	400	tanh	13.605	0.749
30	0.406	400	tanh	13.460	1.021
30	0.438	400	tanh	15.136	1.202
30	0.469	400	tanh	13.917	1.211
30	0.500	400	tanh	13.574	1.538

A.3 Horizontal Configuration Position Hyperparameters

Velocity v_x Sensors	Displacement	Layer Size	Activation	Validation Error	SD
2	0.031	800	tanh	0.083	0.011
2	0.062	800	ReLU	0.085	0.004
2	0.094	800	ReLU	0.084	0.004
2	0.125	800	ReLU	0.084	0.007
2	0.156	800	ReLU	0.084	0.007
2	0.188	800	tanh	0.086	0.008
2	0.219	800	ReLU	0.085	0.006
2	0.250	800	ReLU	0.084	0.007
2	0.281	800	ReLU	0.084	0.007
2	0.312	800	ReLU	0.083	0.007
2	0.344	800	ReLU	0.085	0.006
2	0.375	800	ReLU	0.084	0.006
2	0.406	800	tanh	0.081	0.007
2	0.438	800	ReLU	0.083	0.007
2	0.469	800	ReLU	0.083	0.005
2	0.500	800	tanh	0.083	0.009
3	0.031	800	ReLU	0.078	0.006
3	0.062	800	ReLU	0.077	0.005
3	0.094	800	ReLU	0.078	0.005
3	0.125	800	ReLU	0.077	0.003
3	0.156	800	ReLU	0.080	0.007
3	0.188	800	tanh	0.076	0.009
3	0.219	800	tanh	0.078	0.008
3	0.250	800	tanh	0.078	0.008
3	0.281	800	ReLU	0.078	0.005
3	0.312	800	tanh	0.078	0.008
3	0.344	800	tanh	0.081	0.012
3	0.375	800	tanh	0.080	0.008
3	0.406	800	ReLU	0.078	0.006
3	0.438	800	ReLU	0.080	0.006
3	0.469	800	ReLU	0.077	0.006
3	0.500	800	ReLU	0.080	0.007
4	0.031	800	tanh	0.078	0.009
4	0.062	800	ReLU	0.076	0.006
4	0.094	800	ReLU	0.080	0.004
4	0.125	800	ReLU	0.079	0.008
4	0.156	800	ReLU	0.076	0.005
4	0.188	800	ReLU	0.075	0.006
4	0.219	800	tanh	0.078	0.005
4	0.250	800	ReLU	0.077	0.005
4	0.281	800	ReLU	0.076	0.005
4	0.312	800	ReLU	0.076	0.005
4	0.344	800	ReLU	0.077	0.007
4	0.375	800	ReLU	0.077	0.005

4	0.406	800	ReLU	0.077	0.005
4	0.438	800	tanh	0.077	0.009
4	0.469	800	ReLU	0.077	0.003
4	0.500	800	tanh	0.077	0.004
5	0.031	800	tanh	0.076	0.007
5	0.062	800	ReLU	0.077	0.007
5	0.094	800	tanh	0.076	0.009
5	0.125	800	tanh	0.075	0.007
5	0.156	800	tanh	0.075	0.005
5	0.188	800	ReLU	0.076	0.004
5	0.219	800	tanh	0.076	0.007
5	0.250	800	ReLU	0.076	0.005
5	0.281	800	ReLU	0.077	0.006
5	0.312	800	ReLU	0.077	0.005
5	0.344	800	tanh	0.075	0.007
5	0.375	800	ReLU	0.075	0.004
5	0.406	800	ReLU	0.076	0.004
5	0.438	800	ReLU	0.076	0.006
5	0.469	800	ReLU	0.077	0.004
5	0.500	800	ReLU	0.076	0.006
6	0.031	800	tanh	0.076	0.007
6	0.062	800	tanh	0.076	0.007
6	0.094	800	ReLU	0.076	0.004
6	0.125	800	ReLU	0.076	0.007
6	0.156	800	ReLU	0.076	0.006
6	0.188	800	ReLU	0.076	0.005
6	0.219	800	ReLU	0.075	0.004
6	0.250	800	ReLU	0.076	0.002
6	0.281	800	tanh	0.078	0.007
6	0.312	800	ReLU	0.077	0.003
6	0.344	800	ReLU	0.076	0.005
6	0.375	800	ReLU	0.075	0.004
6	0.406	800	tanh	0.077	0.005
6	0.438	800	ReLU	0.074	0.005
6	0.469	800	ReLU	0.076	0.004
6	0.500	800	ReLU	0.077	0.005
7	0.031	800	ReLU	0.076	0.005
7	0.062	800	tanh	0.075	0.011
7	0.094	800	ReLU	0.077	0.004
7	0.125	800	ReLU	0.075	0.003
7	0.156	800	ReLU	0.076	0.005
7	0.188	800	ReLU	0.077	0.004
7	0.219	800	tanh	0.074	0.006
7	0.250	800	tanh	0.076	0.007
7	0.281	800	ReLU	0.073	0.006
7	0.312	800	tanh	0.075	0.007
7	0.344	800	tanh	0.071	0.007

7	0.375	800	ReLU	0.074	0.008
7	0.406	800	tanh	0.073	0.007
7	0.438	800	ReLU	0.075	0.005
7	0.469	800	tanh	0.074	0.006
7	0.500	800	ReLU	0.075	0.007
8	0.031	800	ReLU	0.075	0.005
8	0.062	800	ReLU	0.075	0.005
8	0.094	800	tanh	0.074	0.008
8	0.125	800	ReLU	0.074	0.005
8	0.156	800	ReLU	0.078	0.005
8	0.188	800	tanh	0.077	0.006
8	0.219	800	ReLU	0.074	0.005
8	0.250	800	ReLU	0.074	0.003
8	0.281	800	ReLU	0.077	0.004
8	0.312	800	ReLU	0.076	0.003
8	0.344	800	tanh	0.075	0.010
8	0.375	800	ReLU	0.075	0.006
8	0.406	800	tanh	0.075	0.004
8	0.438	800	ReLU	0.076	0.005
8	0.469	800	ReLU	0.073	0.004
8	0.500	800	ReLU	0.075	0.005
9	0.031	800	ReLU	0.077	0.007
9	0.062	800	tanh	0.076	0.006
9	0.094	800	tanh	0.073	0.007
9	0.125	800	ReLU	0.077	0.005
9	0.156	800	ReLU	0.076	0.004
9	0.188	800	ReLU	0.076	0.007
9	0.219	800	tanh	0.076	0.008
9	0.250	800	ReLU	0.077	0.005
9	0.281	800	ReLU	0.075	0.005
9	0.312	800	ReLU	0.075	0.005
9	0.344	800	tanh	0.075	0.006
9	0.375	800	tanh	0.076	0.005
9	0.406	800	ReLU	0.076	0.003
9	0.438	800	ReLU	0.075	0.004
9	0.469	800	tanh	0.074	0.008
9	0.500	800	tanh	0.075	0.008
10	0.031	800	tanh	0.076	0.005
10	0.062	800	ReLU	0.074	0.006
10	0.094	800	tanh	0.074	0.008
10	0.125	800	tanh	0.076	0.008
10	0.156	800	ReLU	0.076	0.004
10	0.188	800	ReLU	0.075	0.008
10	0.219	800	tanh	0.075	0.004
10	0.250	800	ReLU	0.075	0.005
10	0.281	800	ReLU	0.075	0.006
10	0.312	800	ReLU	0.075	0.006

10	0.344	800	ReLU	0.076	0.007
10	0.375	800	tanh	0.077	0.008
10	0.406	800	ReLU	0.074	0.005
10	0.438	800	tanh	0.073	0.007
10	0.469	800	ReLU	0.076	0.004
10	0.500	800	tanh	0.074	0.008
11	0.031	800	ReLU	0.077	0.006
11	0.062	800	tanh	0.073	0.007
11	0.094	800	tanh	0.075	0.010
11	0.125	800	ReLU	0.074	0.007
11	0.156	800	ReLU	0.073	0.007
11	0.188	800	tanh	0.075	0.008
11	0.219	800	tanh	0.073	0.008
11	0.250	800	tanh	0.074	0.008
11	0.281	800	ReLU	0.075	0.005
11	0.312	800	ReLU	0.074	0.007
11	0.344	800	ReLU	0.077	0.005
11	0.375	800	tanh	0.073	0.006
11	0.406	800	ReLU	0.075	0.005
11	0.438	800	tanh	0.078	0.012
11	0.469	800	tanh	0.077	0.006
11	0.500	800	tanh	0.074	0.008
12	0.031	800	tanh	0.075	0.010
12	0.062	800	ReLU	0.076	0.005
12	0.094	800	ReLU	0.076	0.004
12	0.125	800	tanh	0.076	0.007
12	0.156	800	ReLU	0.077	0.004
12	0.188	800	ReLU	0.074	0.007
12	0.219	800	tanh	0.075	0.007
12	0.250	800	ReLU	0.076	0.004
12	0.281	800	ReLU	0.074	0.005
12	0.312	800	tanh	0.074	0.007
12	0.344	800	ReLU	0.075	0.006
12	0.375	800	ReLU	0.075	0.004
12	0.406	800	tanh	0.073	0.010
12	0.438	800	tanh	0.075	0.008
12	0.469	800	ReLU	0.074	0.003
12	0.500	800	ReLU	0.075	0.006
13	0.031	800	ReLU	0.076	0.006
13	0.062	800	ReLU	0.075	0.005
13	0.094	800	tanh	0.075	0.004
13	0.125	800	tanh	0.075	0.006
13	0.156	800	tanh	0.073	0.007
13	0.188	800	ReLU	0.076	0.006
13	0.219	800	tanh	0.075	0.005
13	0.250	800	tanh	0.076	0.007
13	0.281	800	tanh	0.078	0.006

13	0.312	800	tanh	0.076	0.006
13	0.344	800	tanh	0.077	0.007
13	0.375	800	ReLU	0.076	0.005
13	0.406	800	tanh	0.077	0.006
13	0.438	800	ReLU	0.075	0.005
13	0.469	800	tanh	0.075	0.006
13	0.500	800	ReLU	0.074	0.006
14	0.031	800	ReLU	0.075	0.005
14	0.062	800	tanh	0.073	0.005
14	0.094	800	tanh	0.073	0.009
14	0.125	800	tanh	0.075	0.010
14	0.156	800	tanh	0.074	0.010
14	0.188	800	ReLU	0.076	0.005
14	0.219	800	ReLU	0.075	0.005
14	0.250	800	tanh	0.078	0.009
14	0.281	800	tanh	0.074	0.010
14	0.312	800	tanh	0.075	0.011
14	0.344	800	ReLU	0.076	0.004
14	0.375	800	ReLU	0.074	0.004
14	0.406	800	tanh	0.075	0.008
14	0.438	800	ReLU	0.075	0.006
14	0.469	800	tanh	0.074	0.009
14	0.500	800	ReLU	0.076	0.007
15	0.031	800	tanh	0.073	0.004
15	0.062	800	tanh	0.078	0.012
15	0.094	800	tanh	0.078	0.010
15	0.125	800	ReLU	0.076	0.004
15	0.156	800	tanh	0.075	0.010
15	0.188	800	ReLU	0.078	0.006
15	0.219	800	ReLU	0.077	0.006
15	0.250	800	ReLU	0.074	0.004
15	0.281	800	ReLU	0.075	0.005
15	0.312	800	tanh	0.076	0.005
15	0.344	800	tanh	0.076	0.005
15	0.375	800	tanh	0.075	0.006
15	0.406	800	tanh	0.076	0.007
15	0.438	800	tanh	0.073	0.007
15	0.469	800	tanh	0.075	0.007
15	0.500	800	tanh	0.076	0.008
16	0.031	800	tanh	0.074	0.008
16	0.062	800	tanh	0.076	0.007
16	0.094	800	tanh	0.074	0.008
16	0.125	800	ReLU	0.074	0.005
16	0.156	800	tanh	0.075	0.009
16	0.188	800	tanh	0.075	0.009
16	0.219	800	tanh	0.074	0.007
16	0.250	800	tanh	0.074	0.008

16	0.281	800	tanh	0.074	0.006
16	0.312	800	ReLU	0.078	0.005
16	0.344	800	ReLU	0.076	0.006
16	0.375	800	tanh	0.078	0.010
16	0.406	800	tanh	0.075	0.008
16	0.438	800	ReLU	0.074	0.004
16	0.469	800	tanh	0.071	0.007
16	0.500	800	tanh	0.077	0.010
17	0.031	800	tanh	0.076	0.009
17	0.062	800	ReLU	0.076	0.006
17	0.094	800	tanh	0.078	0.009
17	0.125	800	tanh	0.077	0.008
17	0.156	800	ReLU	0.076	0.005
17	0.188	800	tanh	0.075	0.010
17	0.219	800	ReLU	0.076	0.007
17	0.250	800	ReLU	0.076	0.005
17	0.281	800	tanh	0.073	0.007
17	0.312	800	tanh	0.079	0.011
17	0.344	800	ReLU	0.076	0.006
17	0.375	800	ReLU	0.078	0.005
17	0.406	800	tanh	0.079	0.008
17	0.438	800	tanh	0.078	0.006
17	0.469	800	ReLU	0.078	0.004
17	0.500	800	ReLU	0.077	0.005
18	0.031	800	tanh	0.074	0.013
18	0.062	800	tanh	0.077	0.015
18	0.094	800	tanh	0.077	0.012
18	0.125	800	tanh	0.075	0.009
18	0.156	800	tanh	0.077	0.009
18	0.188	800	tanh	0.076	0.010
18	0.219	800	tanh	0.075	0.009
18	0.250	800	tanh	0.075	0.009
18	0.281	800	tanh	0.077	0.010
18	0.312	800	tanh	0.074	0.009
18	0.344	800	tanh	0.076	0.008
18	0.375	800	tanh	0.075	0.008
18	0.406	800	tanh	0.076	0.008
18	0.438	800	tanh	0.077	0.009
18	0.469	800	tanh	0.077	0.010
18	0.500	800	tanh	0.077	0.010
19	0.031	800	tanh	0.075	0.009
19	0.062	800	tanh	0.078	0.008
19	0.094	800	ReLU	0.078	0.005
19	0.125	800	ReLU	0.076	0.007
19	0.156	800	tanh	0.077	0.008
19	0.188	800	ReLU	0.077	0.005
19	0.219	800	tanh	0.076	0.013

19	0.250	800	tanh	0.074	0.007
19	0.281	800	tanh	0.079	0.011
19	0.312	800	ReLU	0.079	0.007
19	0.344	800	tanh	0.080	0.011
19	0.375	800	tanh	0.079	0.012
19	0.406	800	tanh	0.077	0.008
19	0.438	800	ReLU	0.079	0.004
19	0.469	800	tanh	0.077	0.010
19	0.500	800	tanh	0.077	0.010
20	0.031	800	tanh	0.077	0.010
20	0.062	800	tanh	0.075	0.010
20	0.094	800	tanh	0.076	0.009
20	0.125	800	tanh	0.078	0.011
20	0.156	800	tanh	0.078	0.009
20	0.188	800	tanh	0.075	0.008
20	0.219	800	tanh	0.079	0.009
20	0.250	800	tanh	0.077	0.012
20	0.281	800	tanh	0.078	0.012
20	0.312	800	ReLU	0.081	0.005
20	0.344	800	tanh	0.077	0.008
20	0.375	800	tanh	0.076	0.005
20	0.406	800	tanh	0.078	0.012
20	0.438	800	tanh	0.075	0.008
20	0.469	800	tanh	0.079	0.006
20	0.500	800	tanh	0.077	0.007
21	0.031	800	tanh	0.075	0.008
21	0.062	800	tanh	0.076	0.015
21	0.094	800	tanh	0.077	0.008
21	0.125	800	tanh	0.077	0.009
21	0.156	800	tanh	0.077	0.012
21	0.188	800	tanh	0.075	0.009
21	0.219	800	tanh	0.075	0.009
21	0.250	800	tanh	0.076	0.006
21	0.281	800	tanh	0.078	0.010
21	0.312	800	tanh	0.075	0.005
21	0.344	800	tanh	0.076	0.009
21	0.375	800	tanh	0.077	0.005
21	0.406	800	tanh	0.077	0.008
21	0.438	800	tanh	0.077	0.008
21	0.469	800	tanh	0.076	0.012
21	0.500	800	tanh	0.076	0.009
22	0.031	800	tanh	0.078	0.014
22	0.062	800	tanh	0.075	0.010
22	0.094	800	tanh	0.077	0.009
22	0.125	800	tanh	0.078	0.009
22	0.156	800	tanh	0.078	0.011
22	0.188	800	tanh	0.078	0.011

22	0.219	800	tanh	0.077	0.008
22	0.250	800	tanh	0.076	0.009
22	0.281	800	tanh	0.074	0.009
22	0.312	800	tanh	0.081	0.012
22	0.344	800	tanh	0.076	0.009
22	0.375	800	tanh	0.077	0.012
22	0.406	800	tanh	0.080	0.009
22	0.438	800	ReLU	0.080	0.005
22	0.469	800	tanh	0.078	0.015
22	0.500	800	tanh	0.078	0.009
23	0.031	800	tanh	0.077	0.014
23	0.062	800	tanh	0.077	0.010
23	0.094	800	ReLU	0.081	0.006
23	0.125	800	tanh	0.079	0.011
23	0.156	800	tanh	0.078	0.012
23	0.188	800	tanh	0.077	0.010
23	0.219	800	tanh	0.080	0.009
23	0.250	800	tanh	0.076	0.010
23	0.281	800	tanh	0.080	0.011
23	0.312	800	tanh	0.081	0.009
23	0.344	800	tanh	0.077	0.009
23	0.375	800	tanh	0.079	0.014
23	0.406	800	tanh	0.078	0.010
23	0.438	800	tanh	0.078	0.008
23	0.469	800	tanh	0.077	0.010
23	0.500	800	tanh	0.079	0.013
24	0.031	800	tanh	0.080	0.013
24	0.062	800	tanh	0.079	0.007
24	0.094	800	tanh	0.077	0.009
24	0.125	800	tanh	0.076	0.013
24	0.156	800	tanh	0.080	0.013
24	0.188	800	tanh	0.079	0.012
24	0.219	800	tanh	0.078	0.004
24	0.250	800	tanh	0.078	0.011
24	0.281	800	tanh	0.080	0.010
24	0.312	800	tanh	0.077	0.008
24	0.344	800	tanh	0.079	0.008
24	0.375	800	tanh	0.077	0.012
24	0.406	800	tanh	0.078	0.008
24	0.438	800	tanh	0.080	0.009
24	0.469	800	tanh	0.079	0.008
24	0.500	800	tanh	0.074	0.008
25	0.031	800	tanh	0.077	0.010
25	0.062	800	tanh	0.076	0.011
25	0.094	800	tanh	0.079	0.008
25	0.125	800	tanh	0.077	0.011
25	0.156	800	tanh	0.078	0.009

25	0.188	800	tanh	0.081	0.014
25	0.219	800	tanh	0.080	0.010
25	0.250	800	tanh	0.080	0.010
25	0.281	800	tanh	0.079	0.011
25	0.312	800	tanh	0.078	0.009
25	0.344	800	tanh	0.077	0.011
25	0.375	800	tanh	0.075	0.008
25	0.406	800	tanh	0.080	0.013
25	0.438	800	tanh	0.077	0.008
25	0.469	800	tanh	0.079	0.011
25	0.500	800	ReLU	0.082	0.009
26	0.031	800	tanh	0.085	0.014
26	0.062	800	ReLU	0.085	0.004
26	0.094	800	tanh	0.083	0.016
26	0.125	800	tanh	0.084	0.011
26	0.156	800	tanh	0.083	0.013
26	0.188	800	tanh	0.082	0.012
26	0.219	800	tanh	0.085	0.010
26	0.250	800	tanh	0.082	0.012
26	0.281	800	tanh	0.080	0.011
26	0.312	800	tanh	0.082	0.009
26	0.344	800	ReLU	0.087	0.006
26	0.375	800	tanh	0.080	0.010
26	0.406	800	tanh	0.080	0.012
26	0.438	800	tanh	0.080	0.010
26	0.469	800	tanh	0.086	0.017
26	0.500	800	tanh	0.080	0.012
27	0.031	800	tanh	0.082	0.009
27	0.062	800	tanh	0.083	0.009
27	0.094	800	tanh	0.078	0.012
27	0.125	800	tanh	0.085	0.018
27	0.156	800	tanh	0.081	0.010
27	0.188	800	tanh	0.081	0.008
27	0.219	800	tanh	0.085	0.010
27	0.250	800	tanh	0.085	0.012
27	0.281	800	tanh	0.085	0.011
27	0.312	800	tanh	0.080	0.012
27	0.344	800	tanh	0.080	0.008
27	0.375	800	tanh	0.084	0.011
27	0.406	800	tanh	0.085	0.015
27	0.438	800	tanh	0.085	0.013
27	0.469	800	tanh	0.085	0.017
27	0.500	800	tanh	0.082	0.011
28	0.031	800	tanh	0.084	0.013
28	0.062	800	tanh	0.085	0.018
28	0.094	800	tanh	0.089	0.016
28	0.125	800	tanh	0.089	0.012

28	0.156	800	tanh	0.085	0.010
28	0.188	800	tanh	0.087	0.011
28	0.219	800	tanh	0.088	0.015
28	0.250	800	tanh	0.089	0.014
28	0.281	800	tanh	0.082	0.012
28	0.312	800	tanh	0.086	0.016
28	0.344	800	tanh	0.089	0.010
28	0.375	800	tanh	0.086	0.018
28	0.406	800	tanh	0.091	0.014
28	0.438	800	tanh	0.084	0.012
28	0.469	800	tanh	0.089	0.017
28	0.500	800	tanh	0.084	0.014
29	0.031	800	tanh	0.098	0.020
29	0.062	800	tanh	0.095	0.013
29	0.094	800	tanh	0.096	0.011
29	0.125	800	tanh	0.101	0.013
29	0.156	800	tanh	0.095	0.008
29	0.188	800	tanh	0.097	0.010
29	0.219	800	tanh	0.097	0.022
29	0.250	800	tanh	0.092	0.016
29	0.281	800	tanh	0.098	0.014
29	0.312	800	tanh	0.094	0.015
29	0.344	800	tanh	0.097	0.019
29	0.375	800	tanh	0.101	0.020
29	0.406	800	tanh	0.096	0.011
29	0.438	800	tanh	0.093	0.017
29	0.469	800	tanh	0.092	0.010
29	0.500	800	tanh	0.096	0.011
30	0.031	800	ReLU	0.129	0.012
30	0.062	800	ReLU	0.128	0.014
30	0.094	800	tanh	0.127	0.028
30	0.125	800	ReLU	0.124	0.015
30	0.156	800	ReLU	0.124	0.011
30	0.188	800	ReLU	0.128	0.011
30	0.219	800	ReLU	0.128	0.010
30	0.250	800	tanh	0.129	0.021
30	0.281	800	tanh	0.128	0.031
30	0.312	800	ReLU	0.127	0.012
30	0.344	800	ReLU	0.130	0.007
30	0.375	800	tanh	0.123	0.016
30	0.406	800	ReLU	0.128	0.010
30	0.438	800	tanh	0.124	0.023
30	0.469	800	tanh	0.121	0.018
30	0.500	800	tanh	0.125	0.039

A.4 Horizontal Configuration Orientation Hyperparameters

Velocity v_x Sensors	Displacement	Layer Size	Activation	Validation Error	SD
2	0.031	1200	tanh	3.501	0.329
2	0.062	800	tanh	3.419	0.721
2	0.094	800	tanh	3.367	0.794
2	0.125	800	tanh	3.314	0.434
2	0.156	800	tanh	3.264	0.308
2	0.188	800	tanh	3.272	0.539
2	0.219	800	tanh	3.205	0.583
2	0.250	1200	tanh	3.372	0.576
2	0.281	800	tanh	3.280	0.350
2	0.312	800	tanh	3.366	0.819
2	0.344	800	tanh	3.289	0.526
2	0.375	800	tanh	3.326	0.411
2	0.406	800	tanh	3.474	0.586
2	0.438	800	tanh	3.329	0.386
2	0.469	800	tanh	3.266	0.445
2	0.500	800	tanh	3.572	0.564
3	0.031	800	tanh	3.254	0.493
3	0.062	800	tanh	3.145	0.520
3	0.094	800	tanh	3.086	0.453
3	0.125	800	tanh	3.162	0.462
3	0.156	1200	tanh	2.971	0.496
3	0.188	1200	tanh	3.135	0.646
3	0.219	800	tanh	3.080	0.277
3	0.250	800	tanh	3.038	0.261
3	0.281	1200	tanh	3.115	0.558
3	0.312	1200	tanh	3.225	0.534
3	0.344	800	tanh	3.119	0.712
3	0.375	800	tanh	3.162	0.384
3	0.406	800	tanh	2.982	0.389
3	0.438	800	tanh	3.090	0.304
3	0.469	1200	tanh	3.064	0.788
3	0.500	800	tanh	3.179	0.508
4	0.031	800	tanh	3.081	0.429
4	0.062	800	tanh	2.967	0.302
4	0.094	800	tanh	2.950	0.437
4	0.125	800	tanh	3.014	0.383
4	0.156	800	tanh	3.164	0.436
4	0.188	1200	tanh	3.161	0.594
4	0.219	800	tanh	2.977	0.582
4	0.250	1200	tanh	2.907	0.669
4	0.281	800	tanh	3.197	0.443
4	0.312	800	tanh	2.971	0.395
4	0.344	800	tanh	3.001	0.276
4	0.375	800	tanh	2.932	0.431
4	0.406	1200	tanh	3.084	0.482
4	0.438	1200	tanh	2.881	0.400
4	0.469	800	tanh	3.026	0.334

4	0.500	800	tanh	2.988	0.344
5	0.031	800	tanh	3.064	0.614
5	0.062	1200	tanh	2.975	0.426
5	0.094	1200	tanh	3.196	0.470
5	0.125	1200	tanh	2.992	0.446
5	0.156	1200	tanh	2.977	0.414
5	0.188	800	tanh	2.876	0.327
5	0.219	800	tanh	3.029	0.728
5	0.250	800	tanh	3.238	0.341
5	0.281	800	tanh	2.877	0.377
5	0.312	1200	tanh	3.144	0.569
5	0.344	800	tanh	2.979	0.298
5	0.375	800	tanh	2.764	0.231
5	0.406	1200	tanh	2.972	0.259
5	0.438	1200	tanh	3.062	0.287
5	0.469	1200	tanh	2.967	0.597
5	0.500	800	tanh	3.097	0.223
6	0.031	1200	tanh	3.028	0.576
6	0.062	1200	tanh	3.066	0.501
6	0.094	800	tanh	2.832	0.354
6	0.125	800	tanh	2.978	0.389
6	0.156	1200	tanh	2.822	0.514
6	0.188	800	tanh	2.959	0.361
6	0.219	1200	tanh	3.153	0.736
6	0.250	1200	tanh	2.990	0.437
6	0.281	800	tanh	2.922	0.203
6	0.312	800	tanh	3.208	0.459
6	0.344	1200	tanh	3.059	0.672
6	0.375	1200	tanh	3.094	0.508
6	0.406	800	tanh	3.112	0.440
6	0.438	1200	tanh	3.007	0.473
6	0.469	1200	tanh	3.106	0.612
6	0.500	1200	tanh	2.872	0.419
7	0.031	1200	tanh	2.975	0.429
7	0.062	1200	tanh	2.998	0.960
7	0.094	800	tanh	2.871	0.436
7	0.125	1200	tanh	2.915	0.438
7	0.156	1200	tanh	2.809	0.542
7	0.188	800	tanh	2.918	0.434
7	0.219	1200	tanh	2.971	0.431
7	0.250	1200	tanh	2.875	0.457
7	0.281	800	tanh	2.849	0.414
7	0.312	800	tanh	2.968	0.396
7	0.344	1200	tanh	2.876	0.554
7	0.375	800	tanh	2.878	0.275
7	0.406	1200	tanh	2.932	0.605
7	0.438	800	tanh	3.007	0.271

7	0.469	1200	tanh	2.833	0.661
7	0.500	1200	tanh	2.828	0.395
8	0.031	1200	tanh	3.176	0.423
8	0.062	1200	tanh	2.781	0.348
8	0.094	1200	tanh	2.856	0.560
8	0.125	1200	tanh	2.807	0.440
8	0.156	800	tanh	2.935	0.346
8	0.188	1200	tanh	2.906	0.574
8	0.219	1200	tanh	3.038	0.651
8	0.250	800	tanh	2.957	0.382
8	0.281	800	tanh	3.070	0.413
8	0.312	800	tanh	3.003	0.437
8	0.344	1200	tanh	2.728	0.370
8	0.375	800	tanh	2.822	0.310
8	0.406	800	tanh	2.911	0.419
8	0.438	800	tanh	2.988	0.533
8	0.469	800	tanh	2.881	0.286
8	0.500	800	tanh	2.807	0.283
9	0.031	1200	tanh	3.020	0.424
9	0.062	1200	tanh	2.841	0.472
9	0.094	800	tanh	2.958	0.427
9	0.125	1200	tanh	2.761	0.357
9	0.156	800	tanh	2.912	0.516
9	0.188	800	tanh	2.829	0.388
9	0.219	1200	tanh	2.788	0.674
9	0.250	1200	tanh	2.747	0.334
9	0.281	800	tanh	3.010	0.472
9	0.312	1200	tanh	2.934	0.485
9	0.344	1200	tanh	3.014	0.554
9	0.375	800	tanh	2.869	0.360
9	0.406	800	tanh	2.987	0.516
9	0.438	800	tanh	3.046	0.529
9	0.469	1200	tanh	2.681	0.457
9	0.500	1200	tanh	3.040	0.604
10	0.031	800	tanh	3.011	0.195
10	0.062	800	tanh	2.853	0.527
10	0.094	1200	tanh	2.951	0.474
10	0.125	1200	tanh	2.742	0.443
10	0.156	800	tanh	2.779	0.215
10	0.188	800	tanh	2.925	0.384
10	0.219	800	tanh	2.862	0.452
10	0.250	800	tanh	2.922	0.574
10	0.281	1200	tanh	2.869	0.369
10	0.312	1200	tanh	3.077	0.655
10	0.344	1200	tanh	2.868	0.521
10	0.375	800	tanh	2.912	0.416
10	0.406	800	tanh	3.009	0.322

10	0.438	800	tanh	2.923	0.414
10	0.469	800	tanh	2.835	0.306
10	0.500	1200	tanh	2.996	0.492
11	0.031	1200	tanh	2.757	0.510
11	0.062	1200	tanh	2.800	0.496
11	0.094	1200	tanh	2.831	0.629
11	0.125	1200	tanh	2.997	0.677
11	0.156	800	tanh	3.139	0.558
11	0.188	800	tanh	2.806	0.310
11	0.219	800	tanh	2.866	0.547
11	0.250	1200	tanh	2.781	0.673
11	0.281	800	tanh	2.781	0.456
11	0.312	1200	tanh	3.035	0.331
11	0.344	800	tanh	3.008	0.303
11	0.375	1200	tanh	2.859	0.714
11	0.406	1200	tanh	2.899	0.804
11	0.438	1200	tanh	2.844	0.572
11	0.469	1200	tanh	3.013	0.692
11	0.500	1200	tanh	2.981	0.462
12	0.031	1200	tanh	3.112	0.630
12	0.062	1200	tanh	2.884	0.520
12	0.094	1200	tanh	2.730	0.669
12	0.125	1200	tanh	3.007	0.493
12	0.156	800	tanh	2.823	0.389
12	0.188	800	tanh	2.789	0.274
12	0.219	800	tanh	3.079	0.405
12	0.250	1200	tanh	2.917	0.379
12	0.281	800	tanh	2.975	0.415
12	0.312	1200	tanh	2.862	0.358
12	0.344	1200	tanh	2.838	0.314
12	0.375	800	tanh	2.902	0.397
12	0.406	800	tanh	2.906	0.506
12	0.438	800	tanh	2.872	0.372
12	0.469	1200	tanh	2.664	0.487
12	0.500	1200	tanh	2.965	0.524
13	0.031	1200	tanh	2.824	0.700
13	0.062	1200	tanh	2.960	0.527
13	0.094	800	tanh	2.744	0.348
13	0.125	1200	tanh	2.727	0.546
13	0.156	1200	tanh	2.692	0.427
13	0.188	1200	tanh	2.726	0.495
13	0.219	1200	tanh	2.986	0.576
13	0.250	1200	tanh	3.059	0.722
13	0.281	800	tanh	2.996	0.517
13	0.312	800	tanh	2.905	0.507
13	0.344	800	tanh	2.883	0.304
13	0.375	800	tanh	3.014	0.291

13	0.406	800	tanh	3.004	0.505
13	0.438	800	tanh	2.953	0.395
13	0.469	800	tanh	3.025	0.416
13	0.500	800	tanh	3.128	0.220
14	0.031	1200	tanh	2.807	0.658
14	0.062	800	tanh	2.908	0.274
14	0.094	1200	tanh	2.827	0.480
14	0.125	800	tanh	2.795	0.455
14	0.156	800	tanh	2.903	0.493
14	0.188	1200	tanh	2.817	0.605
14	0.219	1200	tanh	2.781	0.534
14	0.250	800	tanh	3.057	0.504
14	0.281	1200	tanh	2.834	0.356
14	0.312	800	tanh	2.827	0.424
14	0.344	800	tanh	2.896	0.446
14	0.375	800	tanh	2.917	0.427
14	0.406	800	tanh	2.727	0.292
14	0.438	800	tanh	3.022	0.682
14	0.469	1200	tanh	2.898	0.688
14	0.500	800	tanh	3.010	0.492
15	0.031	800	tanh	2.956	0.432
15	0.062	1200	tanh	2.860	0.354
15	0.094	800	tanh	3.034	0.507
15	0.125	1200	tanh	2.977	0.598
15	0.156	800	tanh	3.001	0.509
15	0.188	1200	tanh	3.070	0.459
15	0.219	800	tanh	2.766	0.369
15	0.250	1200	tanh	3.037	0.441
15	0.281	800	tanh	2.862	0.436
15	0.312	800	tanh	3.034	0.453
15	0.344	1200	tanh	2.861	0.569
15	0.375	1200	tanh	2.650	0.327
15	0.406	800	tanh	2.951	0.330
15	0.438	800	tanh	2.959	0.366
15	0.469	1200	tanh	2.844	0.603
15	0.500	1200	tanh	2.995	0.345
16	0.031	800	tanh	3.014	0.577
16	0.062	1200	tanh	2.949	0.625
16	0.094	800	tanh	2.932	0.338
16	0.125	800	tanh	2.978	0.456
16	0.156	800	tanh	2.819	0.490
16	0.188	800	tanh	2.720	0.396
16	0.219	800	tanh	2.908	0.572
16	0.250	1200	tanh	2.734	0.722
16	0.281	800	tanh	2.691	0.370
16	0.312	800	tanh	2.970	0.461
16	0.344	1200	tanh	2.968	0.802

16	0.375	1200	tanh	2.942	0.522
16	0.406	800	tanh	2.894	0.392
16	0.438	800	tanh	3.006	0.561
16	0.469	800	tanh	2.921	0.432
16	0.500	800	tanh	2.907	0.360
17	0.031	800	tanh	2.882	0.343
17	0.062	1200	tanh	3.093	0.554
17	0.094	800	tanh	3.080	0.503
17	0.125	1200	tanh	2.888	0.559
17	0.156	800	tanh	2.849	0.330
17	0.188	800	tanh	2.949	0.365
17	0.219	800	tanh	2.957	0.345
17	0.250	800	tanh	3.151	0.549
17	0.281	800	tanh	3.011	0.492
17	0.312	1200	tanh	2.878	0.507
17	0.344	800	tanh	2.999	0.520
17	0.375	800	tanh	2.846	0.397
17	0.406	800	tanh	2.976	0.436
17	0.438	800	tanh	2.930	0.555
17	0.469	800	tanh	2.819	0.411
17	0.500	800	tanh	3.125	0.712
18	0.031	1200	tanh	2.940	0.580
18	0.062	800	tanh	3.062	0.515
18	0.094	800	tanh	2.897	0.557
18	0.125	800	tanh	2.862	0.495
18	0.156	800	tanh	2.785	0.472
18	0.188	1200	tanh	2.862	0.679
18	0.219	800	tanh	2.885	0.497
18	0.250	800	tanh	2.747	0.344
18	0.281	800	tanh	2.891	0.324
18	0.312	800	tanh	2.917	0.280
18	0.344	800	tanh	2.803	0.353
18	0.375	800	tanh	2.985	0.446
18	0.406	1200	tanh	2.873	0.473
18	0.438	1200	tanh	2.775	0.425
18	0.469	800	tanh	3.002	0.396
18	0.500	800	tanh	3.008	0.405
19	0.031	800	tanh	2.937	0.558
19	0.062	800	tanh	3.248	0.634
19	0.094	800	tanh	3.016	0.382
19	0.125	800	tanh	2.877	0.309
19	0.156	800	tanh	3.028	0.536
19	0.188	1200	tanh	2.989	0.438
19	0.219	800	tanh	3.215	0.844
19	0.250	1200	tanh	2.873	0.641
19	0.281	1200	tanh	3.050	0.426
19	0.312	1200	tanh	2.966	0.627

19	0.344	800	tanh	3.159	0.571
19	0.375	1200	tanh	3.162	0.591
19	0.406	800	tanh	2.955	0.595
19	0.438	800	tanh	3.137	0.460
19	0.469	1200	tanh	3.069	0.542
19	0.500	800	tanh	3.007	0.607
20	0.031	1200	tanh	3.092	0.529
20	0.062	800	tanh	2.840	0.350
20	0.094	800	tanh	2.964	0.577
20	0.125	800	tanh	3.038	0.413
20	0.156	800	tanh	2.779	0.270
20	0.188	800	tanh	3.120	0.783
20	0.219	1200	tanh	2.920	0.584
20	0.250	800	tanh	3.002	0.432
20	0.281	800	tanh	2.953	0.548
20	0.312	800	tanh	2.835	0.393
20	0.344	800	tanh	2.804	0.437
20	0.375	800	tanh	3.035	0.722
20	0.406	800	tanh	2.973	0.545
20	0.438	800	tanh	3.105	0.534
20	0.469	800	tanh	2.922	0.457
20	0.500	800	tanh	2.946	0.660
21	0.031	1200	tanh	2.895	0.495
21	0.062	800	tanh	3.001	0.379
21	0.094	800	tanh	3.013	0.302
21	0.125	1200	tanh	3.016	0.574
21	0.156	800	tanh	3.087	0.617
21	0.188	1200	tanh	2.900	0.382
21	0.219	800	tanh	2.883	0.624
21	0.250	800	tanh	2.768	0.305
21	0.281	800	tanh	3.099	0.761
21	0.312	800	tanh	2.771	0.512
21	0.344	800	tanh	2.989	0.335
21	0.375	800	tanh	3.099	0.698
21	0.406	800	tanh	3.180	0.639
21	0.438	800	tanh	2.794	0.469
21	0.469	1200	tanh	3.019	0.612
21	0.500	800	tanh	2.856	0.422
22	0.031	1200	tanh	3.061	0.749
22	0.062	800	tanh	2.995	0.513
22	0.094	800	tanh	2.960	0.346
22	0.125	800	tanh	2.998	0.345
22	0.156	800	tanh	2.993	0.521
22	0.188	800	tanh	3.080	0.616
22	0.219	1200	tanh	3.113	0.799
22	0.250	800	tanh	2.947	0.686
22	0.281	800	tanh	3.094	0.664

22	0.312	800	tanh	2.989	0.513
22	0.344	800	tanh	2.874	0.419
22	0.375	800	tanh	2.846	0.381
22	0.406	1200	tanh	2.883	0.657
22	0.438	800	tanh	2.934	0.507
22	0.469	800	tanh	3.112	0.481
22	0.500	800	tanh	2.935	0.536
23	0.031	1200	tanh	2.897	0.441
23	0.062	800	tanh	2.913	0.556
23	0.094	800	tanh	2.886	0.464
23	0.125	1200	tanh	2.913	0.531
23	0.156	800	tanh	2.854	0.498
23	0.188	1200	tanh	3.014	0.493
23	0.219	800	tanh	2.916	0.556
23	0.250	800	tanh	2.823	0.459
23	0.281	800	tanh	2.990	0.512
23	0.312	800	tanh	2.959	0.674
23	0.344	800	tanh	3.095	0.579
23	0.375	800	tanh	3.005	0.506
23	0.406	1200	tanh	3.076	0.523
23	0.438	800	tanh	2.937	0.421
23	0.469	800	tanh	3.013	0.582
23	0.500	800	tanh	2.935	0.561
24	0.031	800	tanh	3.042	0.710
24	0.062	800	tanh	3.014	0.706
24	0.094	800	tanh	3.001	0.536
24	0.125	800	tanh	3.041	0.476
24	0.156	800	tanh	2.943	0.512
24	0.188	800	tanh	3.120	0.591
24	0.219	800	tanh	2.906	0.588
24	0.250	800	tanh	2.942	0.459
24	0.281	800	tanh	3.028	0.615
24	0.312	800	tanh	2.899	0.367
24	0.344	800	tanh	2.930	0.604
24	0.375	800	tanh	3.029	0.615
24	0.406	800	tanh	2.827	0.691
24	0.438	800	tanh	2.785	0.287
24	0.469	800	tanh	2.971	0.797
24	0.500	800	tanh	3.049	0.477
25	0.031	800	tanh	3.222	0.527
25	0.062	800	tanh	2.993	0.318
25	0.094	800	tanh	3.111	0.430
25	0.125	800	tanh	3.047	0.470
25	0.156	800	tanh	3.233	0.704
25	0.188	800	tanh	3.085	0.464
25	0.219	1200	tanh	3.005	0.408
25	0.250	800	tanh	3.173	0.895

25	0.281	800	tanh	2.986	0.338
25	0.312	800	tanh	3.204	0.728
25	0.344	800	tanh	2.815	0.355
25	0.375	800	tanh	3.163	0.496
25	0.406	800	tanh	2.836	0.443
25	0.438	800	tanh	2.849	0.525
25	0.469	800	tanh	2.861	0.520
25	0.500	800	tanh	2.731	0.493
26	0.031	800	tanh	3.031	0.590
26	0.062	800	tanh	3.378	0.457
26	0.094	800	tanh	3.104	0.599
26	0.125	800	tanh	3.300	0.862
26	0.156	800	tanh	3.088	0.445
26	0.188	800	tanh	2.887	0.297
26	0.219	800	tanh	3.103	0.408
26	0.250	800	tanh	3.268	0.473
26	0.281	800	tanh	2.927	0.518
26	0.312	800	tanh	3.068	0.550
26	0.344	800	tanh	3.187	0.614
26	0.375	800	tanh	3.035	0.493
26	0.406	800	tanh	3.081	0.591
26	0.438	800	tanh	3.166	0.628
26	0.469	800	tanh	3.213	0.502
26	0.500	800	tanh	3.066	0.661
27	0.031	800	tanh	3.142	0.808
27	0.062	800	tanh	3.244	0.790
27	0.094	800	tanh	3.096	0.421
27	0.125	800	tanh	3.298	0.672
27	0.156	800	tanh	3.163	0.841
27	0.188	800	tanh	2.873	0.386
27	0.219	800	tanh	3.227	0.626
27	0.250	800	tanh	3.289	0.686
27	0.281	800	tanh	3.475	0.858
27	0.312	800	tanh	3.282	0.472
27	0.344	800	tanh	3.120	0.626
27	0.375	800	tanh	3.185	0.653
27	0.406	800	tanh	2.905	0.482
27	0.438	800	tanh	3.203	0.645
27	0.469	800	tanh	3.198	0.580
27	0.500	800	tanh	3.137	0.534
28	0.031	800	tanh	3.478	0.732
28	0.062	800	tanh	3.014	0.444
28	0.094	800	tanh	3.333	0.629
28	0.125	800	tanh	3.391	0.708
28	0.156	800	tanh	3.701	0.726
28	0.188	800	tanh	3.271	0.577
28	0.219	800	tanh	3.290	0.882

28	0.250	800	tanh	3.271	0.491
28	0.281	800	tanh	3.209	0.677
28	0.312	800	tanh	3.258	0.642
28	0.344	800	tanh	3.453	0.549
28	0.375	800	tanh	3.228	0.606
28	0.406	800	tanh	3.276	0.790
28	0.438	800	tanh	3.217	0.409
28	0.469	800	tanh	3.226	0.501
28	0.500	800	tanh	3.237	0.754
29	0.031	800	tanh	3.388	0.583
29	0.062	800	tanh	3.649	0.401
29	0.094	800	tanh	3.518	0.640
29	0.125	800	tanh	3.668	0.870
29	0.156	800	tanh	3.609	0.655
29	0.188	800	tanh	3.640	0.401
29	0.219	800	tanh	3.497	0.606
29	0.250	800	tanh	3.625	0.698
29	0.281	800	tanh	3.515	0.708
29	0.312	800	tanh	3.469	0.404
29	0.344	800	tanh	3.701	0.672
29	0.375	800	tanh	3.338	0.606
29	0.406	800	tanh	3.493	0.485
29	0.438	800	tanh	3.457	0.478
29	0.469	800	tanh	3.927	0.624
29	0.500	800	tanh	3.709	0.772
30	0.031	800	tanh	5.066	1.298
30	0.062	800	tanh	4.528	0.744
30	0.094	800	tanh	4.709	0.968
30	0.125	800	tanh	5.369	1.211
30	0.156	800	tanh	5.708	1.019
30	0.188	800	tanh	4.909	1.223
30	0.219	800	tanh	4.774	0.687
30	0.250	800	tanh	4.827	0.997
30	0.281	800	tanh	4.751	1.288
30	0.312	800	tanh	5.209	0.764
30	0.344	800	tanh	4.577	0.777
30	0.375	800	tanh	5.120	0.951
30	0.406	800	tanh	4.746	0.975
30	0.438	800	tanh	4.854	0.756
30	0.469	800	tanh	5.076	1.055
30	0.500	800	tanh	4.802	0.904